Archives of Civil and Mechanical Engineering (2025) 25:72
https://doi.org/10.1007/s43452-025-01127-4

ORIGINAL ARTICLE

Mechanical anchorage system in retrofitting of RC slabs using CFRP rods and concrete jacket

Firas Hassan Saeed[2] · **Farzad Hejazi**[1] · **Raizal Saifulnaz Muhammad Rashid**[2]

Received: 2 September 2024 / Revised: 12 November 2024 / Accepted: 8 January 2025

Abstract

Over the past few decades, the demand for retrofitting reinforced concrete members has risen dramatically. Retrofitting reinforced concrete slabs with carbon-fiber-reinforced polymer (CFRP) rods and ultra-high-performance-fiber-reinforced-concrete (UHPFRC) jackets is the one of significantly effective techniques. However, the main challenge of employing CFRP rods and UHPFRC jackets technique to strengthen existing reinforced concrete members is the efficiency of using CFRP rods and the debonding issue between old and fresh new concrete jacketing. Debonding mostly occurs between CFRP rods and old concrete, as well as the surfaces of old and new concrete, and is especially prevalent when the slab is subjected to daily repetitive loads such as cyclic loads. In this study, a new retrofitting system utilizing a mechanical anchor system was proposed to improve the bond between the UHPFRC layer and existing slab. This mechanical system incorporates an expandable anchorage bolt and steel plates. Therefore, a benchmark RC slab and two retrofitted RC slabs were experimentally tested under a five-point incremental repeated load (cyclic load) employing the dynamic actuator. The influence of embedded CFRP rods into the jacket of UHPFRC on the performance of system were studied. The experimental results showed that the newly proposed approach was significantly effective in preventing early debonding. In addition, the mechanical system played an essential role by improving the attachment between the jacket and the slab, ensuring better load transfer. A new proposed retrofitting technique improved the capacity of slabs from 164 to 298kN, illustrating an improvement of over 82%. On the other hand, the FE models have been developed to provide both practical validation and deeper analytical insights, ensuring a comprehensive evaluation of the proposed retrofitting system. Experimental data were used to validate the results of the finite-element models, which showed good agreement and high accuracy. Finally, a parametric study was executed to evaluate the impact of various parameters on the performance and efficacy of the new suggested strengthening technique, and to optimize the proposed system parameters, including the diameter of bolts, a normal strength concrete (NSC) jacket with various grades rather than the UHPFRC, applying the proposed retrofitting technique on a compressive side instead of a tension zone, and rebar steel of varying diameters in the jacket instead of CFRP rods. Findings indicated (parametric study) that using anchor bolts with a diameter greater than 12 mm improved the slabs' ultimate load capacity.

Keywords Slab · CFRP rods · UHPFRC · Cyclic load · Mechanical anchor system · Interface model · Finite element method

1 Introduction

Recently, ultra-high-performance fiber reinforced concrete (UHPFRC) has been considered one of the innovative solutions for reinforcement and rehabilitating concrete structures due to its unique properties such as high compressive, and tensile strength, ductility, good durability, and low permeability [1–7]. The long-term durability of concrete structures is a significant aspect of their sustainability, as improved durability extends their service life, hence optimizing resources and minimizing maintenance efforts. The

✉ Farzad Hejazi
farzad.hejazi@uwe.ac.uk

[1] UWE Bristol: University of the West of England, Bristol, UK

[2] Civil Engineering Department, University Putra Malaysia, Serdang, Malaysia

Published online: 28 January 2025

exceptional durability of UHPFRC has been extensively documented [6–11]. In addition, the UHPFRC is approvingly resistant for environmental impacts like fire, freeze–thaw cycles, and corrosion. This enables it an optimal material for various structural applications, especially for the rehabilitation of concrete structures, and a superior choice for infrastructures requiring extended lifespan in harsh environments [11, 12]. In recent decades, numerous studies have been conducted to examine the behavior of reinforced concrete (RC) members strengthening with UHPFRC, either using experimental or numerical simulation methods [8–13]. However, the majority of these studies applied it as a strengthening layer to existing reinforced concrete members, either through fresh casting or prefabricated layers fixed with epoxy adhesive [14–16]. Paschalis et al. [15] conducted a study that examined the flexural performance of RC beams that were strengthened using a UHPFRC. The study used both reinforced and nonreinforced jacket to strengthen RC beams. Adding a jacket enhanced the reinforced beams' stiffness and load-bearing capacity while delaying the cracks' development. S. Ahmed et al. [17] investigated the behavior of reinforced concrete beams strengthened by the fresh UHPFRC layer in the tension zone. Before the casting of the fresh layer, the tension side of the beams was roughened manually with depths around 2.5–5.0 mm. In addition, a three-dimensional model was performed using a finite-element model. The surface-to-surface contact technique was employed in the FE models to interact the normal concrete NC and UHPFRC. The significant parameters, such as the length of the layer and various thicknesses, were discussed. The results indicated that the strengthened beams showed debonding failure with enhancements in terms of ultimate load, stiffness, and energy absorption. The performance and effectiveness of two various approaches for reinforcing RC beams employing UHPFRC were investigated [18]. The first method involved casting fresh, while the second way involved affixing prefabricated strips to the RC beams with epoxy adhesive. The results demonstrated that the first method had higher bond strength when subjected to shear stress testing. However, [18] developed a three-dimensional (3D) finite-element (FE) model to achieve satisfactory agreement with the results of the laboratory. When modeling concrete and UHPFRC, non-linear behavior was used. Furthermore, a tie constraint was employed to connect the concrete beam to the strengthening layer, supposing a perfect bond. For quasi-static loading, UHPFRC jacketing significantly enhanced stiffness and flexural strength compared to the control beam by 42% and 100%, respectively [19]. J. Yang et al. [20] focused on utilizing steel-reinforced UHPFRC jacket, a GFRP-reinforced, jacket and CFRP mesh to strengthen existing pre-damaged full-scale hollow slab beams. The results were calculated using a numerical investigation and an implicit solver. For the simulation of the RC beam and reinforced layer, the concrete-damaged plasticity model (CDPM) was used. The tie technique was used to represent the interface contact between CFRP mesh and existing concrete. Additionally, the FE model neglects the bond slip between the parts. The outcomes demonstrated an increase in the maximum flexural capacity of the hollow slab beam that was strengthened by a GFRP reinforced and CFRP mesh of 47.1% and 41.2%, respectively. W. Sun et al. [21] developed an FE model and designed an approach for the interface of RC structures strengthened with UHPFRC employing post installed rebars. To simplify the analysis, it was assumed that the bonds between the concrete and the steel reinforcement were perfectly bonded. The concrete around the rebars failed when the distance between post-installed rebars was three times the diameter of the rebar and the layer thickness held little impact on the post installed rebar bond resistance. On the other hand, the FE model was created to investigate the impact thickness of the layer, the ratio of reinforcements, and the spacing of the post-installed rebar on the flexural behaviors of reinforced concrete beams strengthened [12]. The simulation involved utilizing three-dimensional continuum element-8 nodes-reduced integration (C3D8R) for modeling both the UHPC layer and the RC beam. Additionally, reinforcement steel bars were represented in the simulation using truss element-3 dimensional-2 nodes (T3D2). Moreover, the interface regions were modeled using the surface-to-surface contact pairs' technique in the model. Su et al. [12] identified two distinct failure modes during the push-out test: one involving the post-installed steel rebar slipping out, and the other characterized by shear failure of the Normal-Strength Concrete (NSC). In addition, the FE investigation revealed that an increase in the reinforcement ratio within it and the thickness of the layer could significantly enhance the maximum flexural capacity and stiffness of strengthened beams. Hassan et al. [22] reported that using UHPFRC substantially impacted the initial cracking loads on the bottom face of reinforced slabs. Strengthened slabs showed an average increase of 82% in the initial cracking load. At the same time, Hong et al.'s [23] experiments demonstrated that the thickness of the UHPC and the retrofitting type has an impact on the stiffness, failure mode, ductility, and capacity of the beam. Paschalis and Lampropoulos [24] employed dowels connecter between the NSC-UHPFRC to prevent premature debonding. The efficacy of using the jacket on three sides was evaluated. The study observed that using the jackets without connecter dowels was effective until the serviceability limit, when excessive the values of slip led to debonding and decreased beam capacity. Using the dowels improved bonding between two concrete slabs. Furthermore, dowels slowed the formation of cracks. The impact of the strengthening technique, ratio of fiber, and jacket thickness on the shear force of RC beams strengthened with a UHPFRC was studied by Said et al. [25].

The direct pouring it on the beam substrate improved beam ductility, load capacity, and toughness compared to the anchoring method. Increasing the strengthening layer thickness and steel fiber ratio improved the strength of the beams and ductility. Historically, UHPFRC has been applied in different strengthening approaches, including overlays, prefabricated, and jackets. Nevertheless, traditional strengthening systems still face challenges associated with a lack of bond strength and debonding between the existing members and the attached strengthening system [23, 24]. Premature debonding poses a considerable risk to the effectiveness of strengthening systems, especially when exposed to repetitive loads and vibrations. The current retrofitting approach introduces a novel mechanical anchor system designed to improve the bind between the jacket of UHPFRC and the slab, and to effectively and durably overcome the obstacles and limitations of previous strengthening methods, including the issue of premature debonding. This system incorporates CFRP rods, jacketing of the UHPFRC, and an anchorage system (expansion anchor bolts with steel plate). The system's effectiveness was evaluated through experimental testing under half-cyclic load conditions. Two various cases regarding the interaction contact models for the bolt with the UHPFRC and NSC layers were discussed by developing the FEM. Experimental testing allows direct observation of the physical behavior of retrofitted slabs under controlled loading conditions, providing critical empirical data on slab performance, whereas numerical methods enable the simulation of diverse scenarios and conditions that may be infeasible to reproduce in a laboratory environment. Also, the FE models offer both empirical validation and enhanced analytical insights, guaranteeing a thorough assessment of the proposed retrofitting system. Additionally, the study examines the effects of various parameters on the performance of the retrofitted slab. These parameters include the diameters of the anchor bolts, using the NC layer with different grades of concrete instead of UHPFRC, applying the newly proposed retrofitting technique to the compression side instead of the tension zone, and employing steel rebar of differing diameters in the jacket instead of CFRP rods. Accordingly, the behavior of retrofitted slabs regarding the ultimate load, deflection, crack pattern, failure modes, ductility, and elastic stiffness were investigated.

2 Development of the new retrofitting technique for slabs

The new proposed retrofitted method depends mainly on three ingredients: CFRP rods to improve the slab's flexural capacity; UHPFRC jacketing to assure a good bonding with the reinforced-concrete slab, decreasing the probability of the de-bonding or delamination due to its exceptional bonding properties; and also, to protect the CFRP rods from surrounding impacts. Figure 1 shows the all components and details of the proposed strengthening system used in the experimental work. The assembly of the strengthened slab in Fig. 1c, highlights the arrangement of the strengthening system components. The last component is a mechanical anchorage system to bond the CFRP rods and fresh layer of UHPFRC with RC slab, as shown in Fig. 1.

2.1 Materials

2.1.1 UHPFRC

UHPFRC material is a considerable advancement in composite materials that is ideal to reinforce and rehabilitate RC members. In the presently suggested system, the UHPFRC layers are employed to supply the demanded medium to transmit the stresses from an RC slab to CFRP bars and decrease environmental and other influences on CFRP rods. Figure 2 presents the main components of the UHPFRC used in the experimental study. The increased thicker of the UHPFRC provides additional resistance to the punching shear in the slabs [30]. Besides that, increasing the UHPFRC layer thickness reduces the shear stresses in the slab's critical areas [15]. In addition, a reduction in shear stresses may delay or prevent punching shear collapse, thereby improving the durability and performance of the RC slab. As a result, the proposed UHPFRC jacketing thickness was 50 mm, which provides sufficient strengthening to improve slab capacity and performance while also providing the needed cover for the CFRP rods, as depicted in Fig. 1a.

2.1.2 CFRP rods

This investigation used CFRP rods embedded in UHPFRC jacketing to enhance the flexural capacity of the slab specimen. The use of CFRP in this study was prompted by a high elasticity of modulus which induces minor deformation under cyclic loads than reinforcing steel. Furthermore, their lightweight, strength, and resistance to corrosion make the CFRP rods an adaptable and practical alternative for increasing the efficiency and durability of RC members. The CFRP rods were 1440 mm in length and 8 mm in diameter, extending roughly (30 mm) from the mold in two directions, as shown in Fig. 1b. The placement of the CFRP rods has been accurately planned and does not conflict with the layout of the fastener bolts. Besides that, the steel nails were used to attach the CFRP bars to the bottom surface of NC.

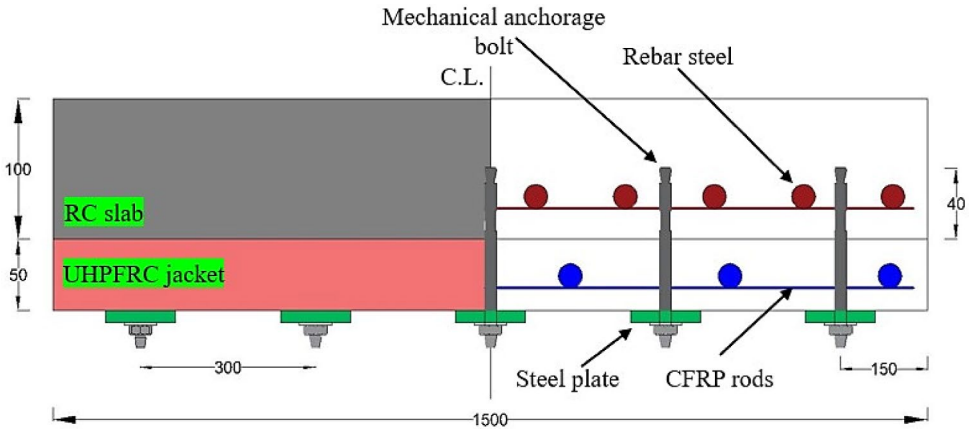

(a) Elevation

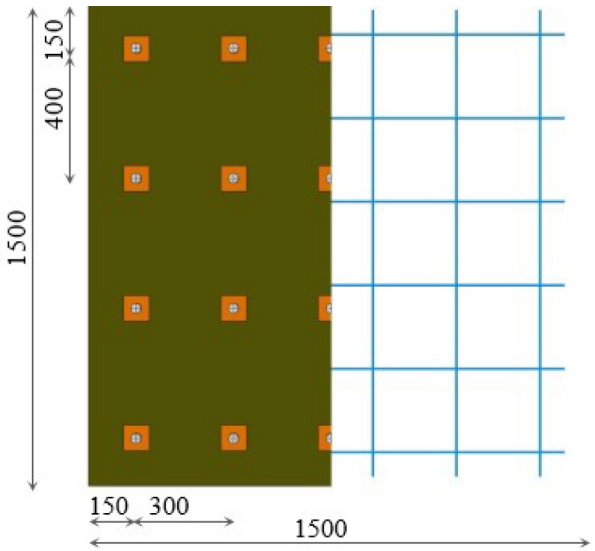

(b) Bottom view

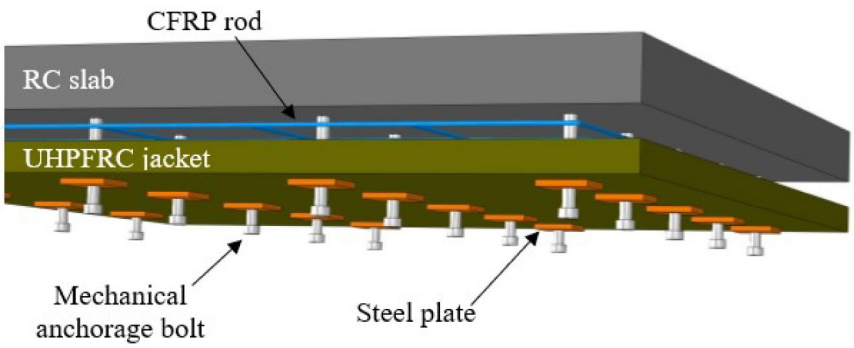

(c) Assembly of strengthened slab

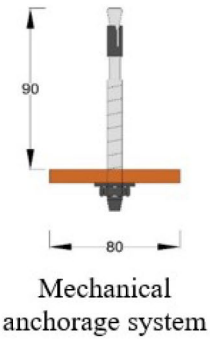

(d) MAS

Fig. 1 Components of the suggested strengthening technique. (Dimensions in mm)

(1) (2) (3)

Fig. 2 Main ingredients of the UHPFRC; (1) steel fiber, (2) admixture for reduction of water, and (3) UHPC premix Dura

2.2 Mechanical systems

2.2.1 Expandable anchor bolts

The mechanical anchor systems in this investigation are comprised of two components: the expandable anchor bolts and steel plate, as shown in Fig. 1d. In the proposed technique, the interface bonding between UHPFRC layer and the existing RC slabs depend on selecting the appropriate anchor bolts to securely bind. Therefore, the material and size of the anchor bolts were chosen based on the manufacturing datasheet [28] due to their high tensile strength and anchorage capacity, which prevent early pull-out or failure under cyclic loading. One anchor bolt is utilized for each steel plate in an anchorage system, as shown in Fig. 1c. These bolts are embedded in the under side of the RC slabs before casting the UHPFRC layer. Expandable anchor bolts 160 mm in length were employed in the experimental work. Of this length, a 40-mm effective length of the bolt was inserted inside the RC slab, and a 50-mm length was implanted in the UHPFRC, as shown in Fig. 1a. The anchor bolt has a diameter of 12 mm, which is the ideal size for the slab and proposed design parameters steel plates and fulfills the necessary resistance requirements. The overlap of stress cones in the reinforced concrete slab, resulting from closely spaced anchor bolts, limits the load-bearing capacity of the fixation and bond strength due to tensile stresses on the bolts [29]. Therefore, the spacing of the anchor bolts was carefully chosen to balance the necessity for effective load transfer and minimizing stress concentrations, as recommended in ACI 318—Anchoring to Concrete [29]. A total of twenty bolts were implanted into the lower surface of each specimen. The space between the two bolts was 400 mm from the center to the center of the other and 300 mm in the opposite direction, as shown in Fig. 1b.

2.2.2 Steel plates

The second ingredient in the proposed anchor system is steel plate, designed in accordance with the ASTM A29 [31]. This standard (ASTM A29) is its capability to offer steel plates with high tensile and yield strength, which is crucial for anchoring the bolt to the jacket. Due to the high loads predicted during cyclic testing, these steel plates need to resist substantial stresses without deforming or failing. The steel plates are designed based on predicted force and stress across a variety of loading situations. This investigation employed steel plates to establish a suitable connection between the UHPFRC layer and the preexisting slab, ensuring sufficient bond strength. However, employing steel plates in this investigation helps to evenly distribute applied loads across the surface of the concrete and prevent localized stress, reducing the probability of premature failure or slab deformation. The combination of expansion bolt and steel plate expanded the anchorage area on the UHPFRC jacket's surface, resulting in more evenly distributed loads and a decreased risk of the anchor bolts slipping. This proposed strengthening system uses a steel plate with dimensions of 80×80 mm and 10 mm thickness. The dimensions of the steel plates were selected based on the previous study of Yang Zhang et al.[32], considering the reduction of system weight through the minimization of plate size. A laser machine was used to create a circular hole in the center of the plate with a diameter that matched that of the expansion anchor bolts.

3 Manufacturing of prototype and conducting experimental test

This study focused on retrofitting a reinforced concrete slab employing CFRP rods with the UHPFRC jacket and mechanical anchor systems. The experimental investigation was carried out using an incremental repeating approach, with each cycle consisting of a pushing phase followed by a releasing phase, and the verification of finite-element specimens (FEM) was also simulated under cyclic loads.

3.1 Geometric details of slab

The study adopted a square-reinforced concrete (RC) slabs with the1300 mm length span and the 100 mm thickness. The reinforced concrete slabs are designed following ACI-318-08 and EC2. A 50-mm thickness of UHPFRC was used as the external strengthening jacket. The experiment investigated three square RC slabs: reference RC slab (benchmark slab), retrofitted RC slab by the jacket of UHPFRC, and strengthened RC slab by an exterior layer of UHPFRC containing incorporated CFRP bars. A 12 mm single-layer steel reinforcement mesh was utilized, with an effective depth of 75 mm. The slabs were constructed and subjected

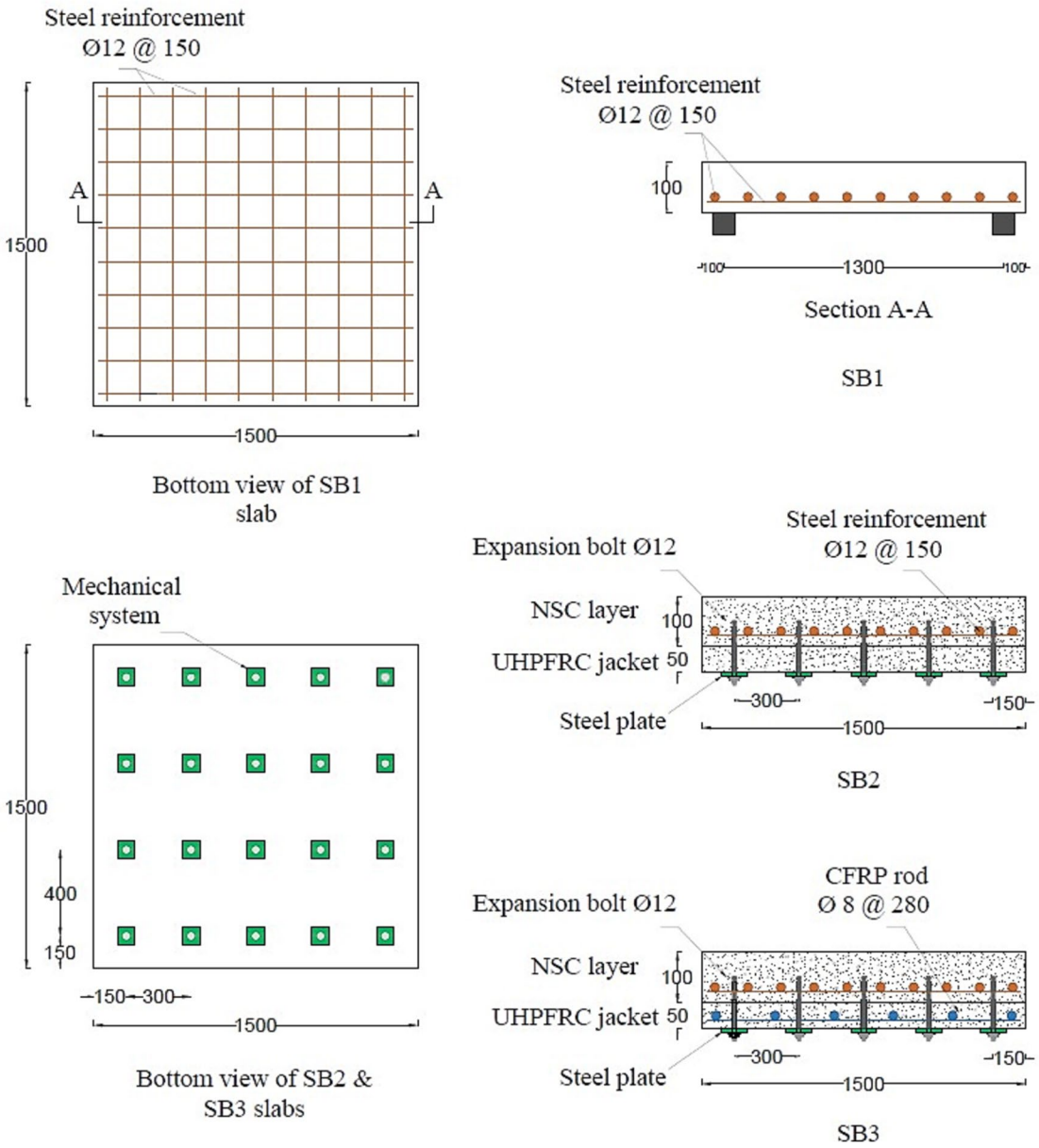

Fig. 3 Details of all specimens

Fig. 4 NC and UHPFRC property evaluation and test

Table 1 Ultimate compressive force for NC and UHPFRC (after 28 days)

Mix	NC	UHPFRC
Cube	Compressive strength (MPa)	
1	34	142.3
2	34.6	144.6
3	35.9	145.7
Average	34.81	144.2

to incremental repeated (half-cycle) loads for experimental testing. Due to financial constraints, the experimental work necessitated limiting the number of specimens. Therefore, extensive simulation analysis was employed to verify the accuracy of the outcomes with FE software. Figure 3 illustrates the primary specifications of geometric slabs.

3.2 Materials properties

Single-patch ready mix concrete provided from the local manufactory was used to cast the slabs with a compressive strength of C30/37. Figure 4 illustrates the preparation of the concrete cubes and testing for the NSC and UHPFRC. Table 1 displays the results of the NSC and UHPFRC compression strength tests after 28 days. Moreover, these values in Table 1 demonstrate that the selected materials align with the study's goal of optimizing structural performance, especially the higher compressive strength of UHPFRC is crucial for increasing the load-bearing capacity and durability of

Table 2 Mixing proportion for UHPFRC ingredients

Item	Quantity (kg/m3)
Dura UHPC premix	560
Admixture for reduction of water	6.833
Steel fiber (0.2 mm diameter, 20 mm length)	42.1 ((2%) by vol.)
Water	48

Table 3 Properties of materials employed in the study

Item	Characteristics	Values
Reinforcing steel	Density (kg/m3)	7850
	Young's modulus of elasticity (GPa)	210
	Poisson's ratio	0.25
	Yield strength (MPa)	600
CFRP rod [34]	Fiber content (%)	> 68%
	Tensile strength (MPa)	2500
	Elasticity modulus (GPa)	153
	Poison's ratio	0.2
Expansion bolt [28]	Tensile strength (MPa)	700
	Yield strength (MPa)	560
	Elasticity modulus (GPa)	206
	Poison's ratio	0.28
Steel plate	Elasticity modulus (GPa)	207
	Poisson's ratio	0.29
	Yield strength (MPa)	425
	Density (kg/m3)	7860
Silicone	Density (kg/m3)	1230
	Elasticity modulus (GPa)	0.0167
	Poisson's ratio	0.21
	Tensile strength (MPa)	7.11
	Adhesive bond strength (MPa)	0.174
	Water absorption	1.52%
Admixture for reduction of water	Density (kg/m3)	1160
	Viscosity (cps)	311
	pH	4.09
	Solid content (%)	48
Steel fiber	Shape	Copper coated micro steel fiber
	Length (mm)	20
	Diameter (mm)	0.05
	Aspect ratio (L/D)	100
	Tensile strength (MPa)	2500

retrofitted slabs, as well as enhancing resistance to cracking and deformation, which is essential in avoiding early failure under repeated loading conditions. An automatic mixer was employed to prepare the UHPFRC mix with a compressive strength of 144 MPa, under ACI 239R-18 [33]. By following this standard, the study ensures that the UHPFRC material employed in the experiment satisfies industry-recognized criteria for quality, durability, and structural performance, owing to extensive recommendations for the application of material. UHPFRC consists of a substantial amount of regular cement, fine sand, steel fibers, micro-silica, water, and admixture for reduction of water, as depicted in Fig. 2. Steel fibers of 20 mm in length were utilized, having a tensile strength exceeding 2500 MPa, as depicted in Table 3. Table 2 provides the mixing proportion of UHPFRC. The slabs were strengthened with ribbed rebar steel. 12 mm-diameter steel bars (B500B) with a yield force of 600 MPa and an elastic modulus of 210GPa were employed (Table 3). The CFRP rods (CarboDur® BC8) employed in this study had a tensile-strength of 2500 MPa, a Young's modulus of 153GPa, and a Poisson's ratio of 0.2 for 8 mm-diameter rods [34], as depicted in Table 3. The mechanical anchor system consisted of steel plate made from S50C steel fabricated in a local workshop and HAS-BW D12 mechanical expandable anchor bolts, [28]. Table 3 displays the properties of all materials used in the study.

3.3 Casting process

3.3.1 Normal concrete

RC slab specimens was fabricated in the material and structural laboratory of the engineering faculty in the University of Putra Malaysia. Figure 5 depicts the primary process for casting the concrete slabs. The slabs were set up for pouring after the reinforcing steel were positioned inside the mold, and the strain gauges were attached to middle of rebar steel, as shown in Fig. 5a. A 5 mm strain gauge was used for both the reinforcing steel and CFRP rods. An additional layer of silicone material was placed as a protective covering on the strain gauges to prevent possible damage to during the casting process.

3.3.2 UHPFRC

Figure 5b shows the process casting of the UHPFRC with a 50 mm thickness, following the attachment expansion bolt on the underside of the RC slabs. Before the application of the UHPFRC jacket, the slab (SB3) was reinforced by incorporating CFRP rods with a diameter of 8 mm. These bars were placed at intervals of 280 mm in two directions. The ingredients of UHPFRC were manually mixed inside the laboratory, as illustrated in Fig. 5c. During the preparation of the UHPFRC material, temperature in the laboratory was roughly 22◦C. Before beginning the mixing, both wet and dry batch ingredients were measured and weighed. The first stage was mixing the dry ingredients of UHPC premix Dura for 2 min to homogenize. After that, add 100% admixture

Fig. 5 Casting concrete slabs and affixing the strengthening system: (**a**) casting the NC; (**b**) separating the steel fiber and mixing the UHPFRC; (**c**) setting the expansion anchorage bolt and casting UHPFRC; (**d**) attaching the steel plate

and 90% water to the mixture for 4 min and the remaining water 10% is added (if needed). In the final stage gradually added the steel fibers into the mix to prevent clumping or fiber balling, providing even distribution with mixing for 2–5 min. Before discharge, the mix should have good rheology and homogeneity.

3.4 Installation mechanical anchorage system

The efficiency of the proposed reinforcement technique depends on the careful selection of suitable mechanical expansion anchor bolts for securely fixing the normal concrete (NC) layer to the UHPFRC jacket. Therefore, the mechanical expandable anchor bolts were used with the determined size to provide a good anchorage with a suitable quantity of bonding strength. Whenever the concrete curing process was completed (after 28 days), the mechanical expansion anchoring bolts were fastened 40 mm depth to the under surface of the NC layer. The effective depth of the expansion anchor bolt inside the NC layer was based on the ACI guide of design anchor for reinforced concrete [35]. Fastening of the mechanical expandable anchor bolts included identifying the designated positions, drilling holes, embedding the bolts with a hammer, and filling the top face of the holes by silicon to avoid ingression of the water, as demonstrated in Fig. 5c. Figure 5d shows the secure attachment of the second part of the mechanical anchor system (steel plate) to the under face of jacket after the UHPFRC hardened (after 28 days).

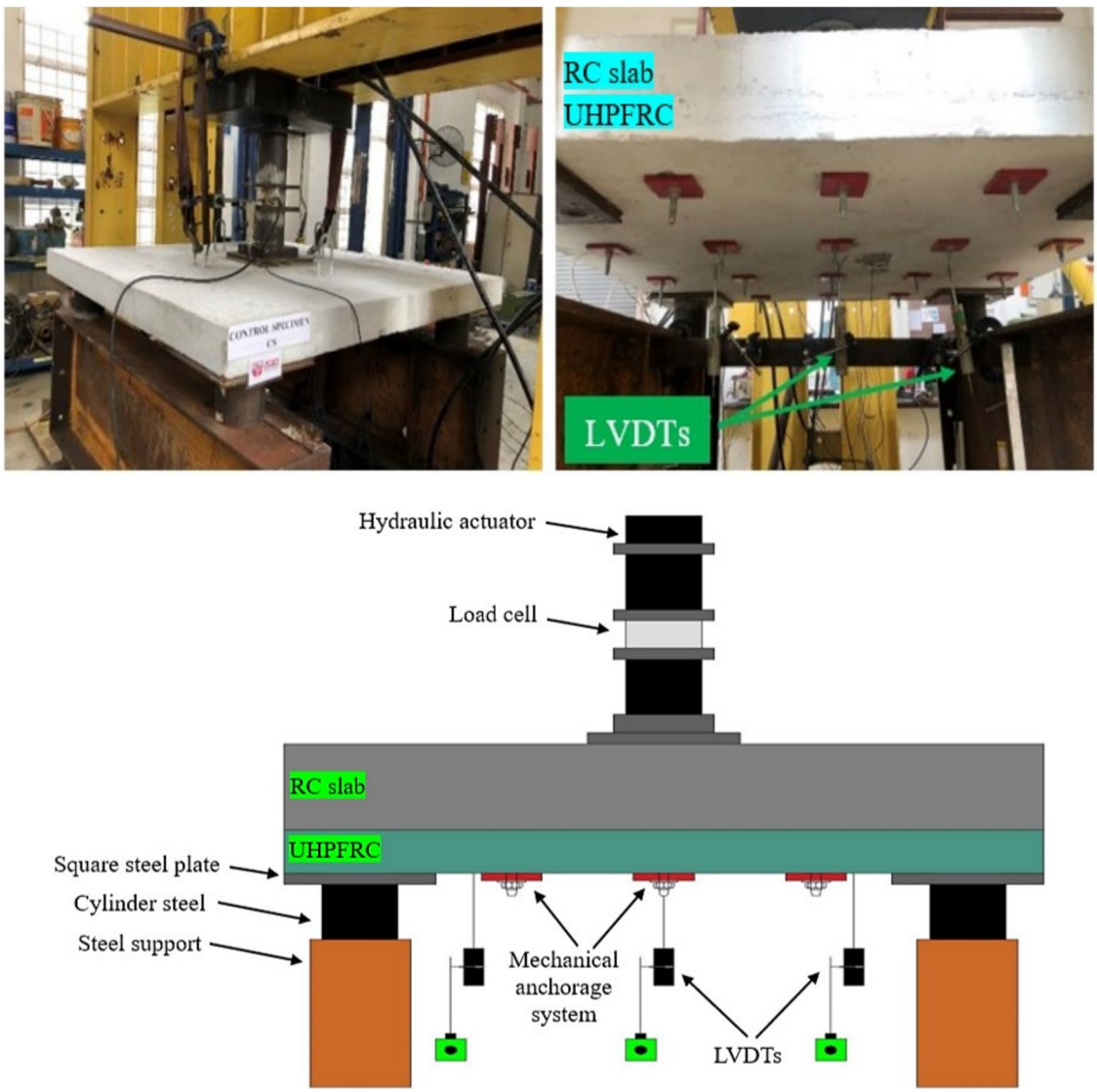

Fig. 6 Test setup for specimens

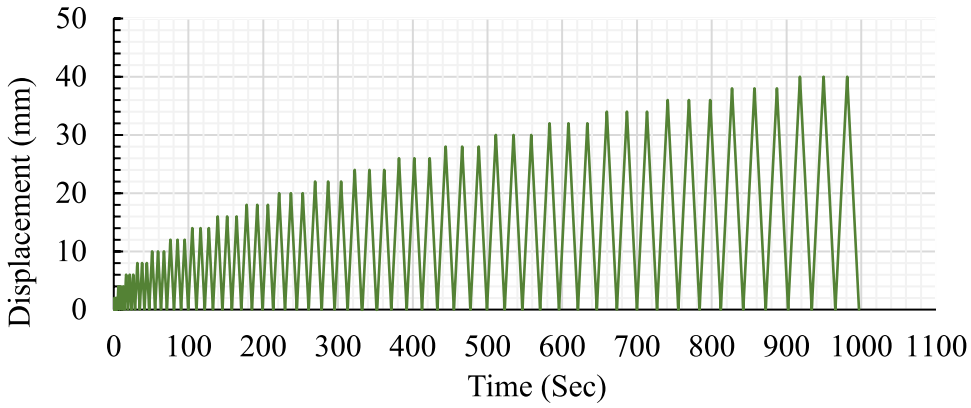

Fig. 7 Protocol of half cyclic loading

3.5 Boundary condition and experimental testing

The repeated incremental load (cyclic-load) was applied using a hydraulic jack (MTS) capable of carrying load over 1000 KN, as shown in Fig. 6. A Shimadzu 4830 servo smart controller was employed to operate the dynamic actuator. The cyclic load is involved using the pushing and releasing phases, allowing the loading cell to back to the initial place at identical rates of loading. The protocol of loading applied to the slab was provided relying on ACI-committee 374.1–05 (ATC-1996), as illustrated in Fig. 7. A predefined displacement history time was supplied and input in controller system. The controller managed the actuator per the designated timeline, simultaneously assessing the necessary load to get the intended movement at each (0.01-s interval). The displacement was orientated downward on the compression side of the slab, starting at 2 mm and accelerating at a rate of 2 mm per cycle until fail occurred. For certain consistent performance throughout the testing procedure, each loading-cycle was replicated three times. The repetition of loading was conducted to confirm the consistent performance of the slab at a loading rate of 2 mm/m. In addition, Fig. 6 illustrates the use of three electronic-linear-variable-differential-transducers (LVDTs) at the center to calculate the deflections of the slab every quarter. Support conditions of the slab were four simply supported square steel plates at all edges of the slab (Fig. 6). Square plates measuring 200 × 200 mm with a clear span of 1300 mm from the center of each other. A steel cylinder with a diameter of 120 mm and a height of 150 mm was placed at the center bottom of each square steel plate. These cylinders transfer the loads to the two H-shaped steel supports, as shown in Fig. 6. In addition, the load application point was on a square plate, located at the top center of the reinforced concrete slabs, as depicted in Fig. 6.

4 Development of finite-element modeling of the proposed new retrofitting system

The major aim of this section is to develop the 3D finite-element (FE) models capable of simulating the cyclic response of the (RC) slabs strengthened employing the CFRP rods with external UHPFRC jacket and mechanical anchor systems. The nonlinear behavior of materials was used in this study by the ABAQUS software [36]. ABAQUS is widely regarded for its advanced abilities in simulating complex material behaviors, making it an ideal option for this analysis and providing accurate modeling of material nonlinearity, like concrete's cracking and crushing under load. The finite-element investigation comprises two primary parts. The first part entails creating slab models with the same characteristics used in the experimental test, whereas the second section is a parametric study for evaluating the efficacy of the new suggested retrofitted method. Two different interaction contact situations between the expandable bolt and NC-UHPFRC layers are examined, as indicated in Table 5.

4.1 Modeling of NSC and UHPFRC

In the present study, a concrete damaged plasticity model [CDPM] was employed to estimate the nonlinear response of NC and UHPFRC under tension and compression. Figure 8 depicts the stress–strain relationship of the NC-UHPFRC in tension and compressive [33, 34]. The relationships stress–strain constitutive of NC under tension and compressive were acquired from the Code of design-concrete-structures (GB 50010–2010) [37], as shown in Fig. 8a. The stress–strain constitutive curves in this standard (GB 50010–2010) account for significant factors such as strain hardening and softening, peak stresses, and the post-peak behavior of NC, which are essential for inserting in the ABAQUS software [CDPM] to capture the realistic behavior of models under loading. This is especially important for dynamic or cyclic loading conditions, where the compressive and tensile responses of the NC can significantly impact the overall performance of the model.

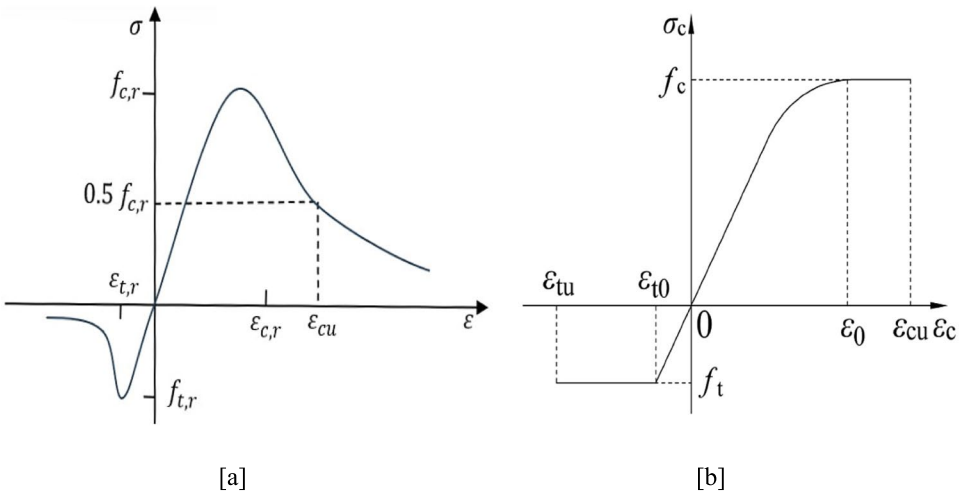

Fig. 8 Uniaxial stress–strain curves in compressive and tension of: [**a**] NC [37] and [**b**] UHPFRC [38]

Table 4 Mechanical characteristics of NSC and UHPFRC employed in the FE models

Type of element	Description	Value
NC	Compressive strength (MPa)	34
	Tensile strength (MPa)	3
	Poisson's ratio	0.2
	Density (kg/m3)	2200
UHPFRC	Compressive strength (MPa)	144
	Tensile strength (MPa)	10.5
	Poisson's ratio	0.2
	Density (kg/m3)	2300

Equations 1 and 4 were used to calculating the compressive and tensile stress–strain of the NC. On the other hand, the uniaxial stress–strain relationship for the UHPFRC was confined using the approach of Jia et al. [38], as displayed in Fig. 8b. The compressive and tensile stress–strain of UHPFRC in the peak region can be determined using Eqs. 5 and 6. According to the ABAQUS software user manual [36], it is recommended to convert the stress–strain relationships for NC and UHPFRC to the relationship of stress–inelastic strain. Equations [7, 8] were employed to compute the inelastic strain. Based on [39], Equations [9, 10] were utilized to calculate the concrete damage parameter for compressive strength and tensile strength in both NSC and UHPFRC. Table 4 displays the mechanical characteristics of the NC and UHPFRC. Additionally, CDP model requires additional parameters to comprehensively define the behavior of concrete material. The [CDPM] for the NC layer and UHPFRC jacket adopted the following parameters: the viscosity value is 0.0001, the dilation degree is 36°, the possibility of flow eccentricities is 0.1, the ratio of the stress of the integral on the tension to the compressive diagonal is 0.667, and the force at yield proportion with similar axial compressive compared to the initial-yield force under unilateral compression is 1.16 [12, 17–36]

$$\sigma = \left(1 - d_t\right) E_c \varepsilon \tag{1}$$

$$d_t = \begin{cases} 1 - \rho_t\left[1.2 - 0.2x^5\right] x \le 1 \\ 1 - \frac{\rho_t}{\alpha_t (x-1)^{1.7} + x} x > 1 \end{cases} \quad x = \frac{\varepsilon}{\varepsilon_{t,r}}; \rho_t = \frac{f_{t,r}}{E_c \varepsilon_{t,r}} \tag{2}$$

$$\sigma = \left(1 - d_c\right) E_c \varepsilon \tag{3}$$

$$d_c = \begin{cases} 1 - \frac{\rho_c n}{n - 1 + x^n} x \le 1 \\ 1 - \frac{\rho_c}{\alpha_c (x-1)^2 + x} x > 1 \end{cases} \quad \rho_c = \frac{f_{c,r}}{E_c \varepsilon_{c,r}}; n = \frac{E_c \varepsilon_{c,r}}{E_c \varepsilon_{c,r} - f_{c,r}}; X = \frac{\varepsilon}{\varepsilon_{c,r}} \tag{4}$$

$$\sigma_{c,c} = \begin{cases} f_c \frac{n\xi - \xi^2}{1 + (n-2)\xi} 0 < \varepsilon \le \varepsilon_0 \\ f_c \varepsilon_0 \le \varepsilon_{c,c} \le \varepsilon_{cu} \end{cases} \quad n = \frac{Ec}{Es}; \xi = \frac{\varepsilon_{cu}}{\varepsilon_0} \tag{5}$$

$$\sigma_{c,t} = \begin{cases} f_t \frac{\varepsilon_t}{\varepsilon_{t0}} 0 < \varepsilon_{c,t} \le \varepsilon_{t0} \\ f_t \varepsilon_{t0} < \varepsilon_{c,t} \le \varepsilon_{tu} \end{cases} \quad \varepsilon_{t0} = \frac{f_t}{Ec}; \quad \varepsilon_{tu} = \frac{30 f_t}{Ec} \tag{6}$$

$$\varepsilon_c^{in} = \varepsilon_c - \sigma_c / E_0 \tag{7}$$

$$\varepsilon_t^{in} = \varepsilon_t - \sigma_t / E_0 \tag{8}$$

$$D_t = 1 - \frac{\sigma_t E_c^{-1}}{\varepsilon_t^{pl}\left(\frac{1}{b_t} - 1\right) + \sigma_t E_c^{-1}} \quad \varepsilon_t^{pl} = b_t\, \varepsilon_t^{in} \tag{9}$$

$$D_c = 1 - \frac{\sigma_c E_c^{-1}}{\varepsilon_c^{pl}\left(\frac{1}{b_c} - 1\right) + \sigma_c E_c^{-1}} \quad \varepsilon_c^{pl} = b_c\, \varepsilon_c^{in} \tag{10}$$

$f_{t,r}$ and $f_{c,r}$ denote the tensile and compressive strength of NC, $\varepsilon_{t,r}$ indicates the NC tensile strain corresponding to $f_{t,r}$, $\varepsilon_{c,r}$ denotes the NC compressive strain at the $f_{c,r}$, E_c indicates the elastic modulus, d_t and d_c indicate the tensile and compressive factor of NC, f_c and f_t denote the compressive and tensile strength of UHPFRC, *Es* denotes the equal secant-modulus at maximum state, ε_{cu} and ε_{tu} denote the ultimate compression and tension strain of UHPFRC, ε_0 and ε_{t0} denote the peak compression tension and strain, D_t and D_c indicate the concrete tension and compressive damages parameters, respectively, σ_c and σ_t indicate the stress in compressive and tension, ε_t^{pl} and ε_c^{pl} denote the plastic-strain linked with the tensile and compression stress, respectively, and $b_c$and b_t are invariant values ranging ($0 < b_c and b_t < 1$).

4.2 Steel rebar, CFRP rod, and mechanical system models

The linear-elastic–plastic model and strain hardening was utilizing in this investigation for the rebar steel. In contrast, the CFRP rods were modeled employed an isotropic linear elastic model until collapse [41]. The mechanical anchorage system included a steel plate and an expansion bolt. The steel plate was modeled using the elastic–plastic approach, whereas the expandable bolts were modeled with a bilinear that includes strain hardening. The modulus of hardening used was [0.01 Es] [42]. Table 3 displays the properties of rebar steel, CFRP rods, and anchor system. Figure 9 depicts the stress–strain relationship that is employed to represent the rebar steel and CFRP rods.

4.3 Element types, mesh, and boundary condition

A 3D homogeneous stress 8-node linear-brick element [C3D8R] with reduced integration is employed to models the NC layer, UHPFRC jacket, and mechanical anchorage system components. This type of element [C3D8R] is crucial, since it effectively simulates the non-linear behavior of concrete under intricate stress situations and the reduced integration approach decreases the computational time while avoiding common simulation issues such as volumetric locking. Conversely, a 2-node-linear 3D truss solid-element [T3D2] represents the reinforcing steel bars and CFRP bars [36]. [T3D2] was utilized due to its effective representation of thin elements (slender members) mostly subjected to axial stress and this type ensures that the material behavior and structural responses are precisely represented without imposing an undue computing load. Figure 10 demonstrates the layout of the models. The mesh size in finite-element modeling directly influences the accuracy as well as the effectiveness of the simulations. A finer mesh is frequently employed in crucial regions, such as the interfaces between disparate materials and places of elevated stress concentration, including load application areas or anchorage zones. These locations necessitate greater precision to adequately delineate stress gradients and potential failure causes. Therefore, the NC, UHPFRC, and mechanical system were defined mesh size of [20 mm], as illustrated in Fig. 10. Regarding the boundary condition, restricted supporting steel plates in three directions on the underside surface. During the loading process, the load was distributed uniformly across the whole top face of the steel plate (loading plate). The half-cyclic amplitude analysis was conducted employing the explicit-dynamic solver to validate the finite-element simulation. The cyclic-displacements were defined based on the amplitude of the half-cyclic, as illustrated in Fig. 7.

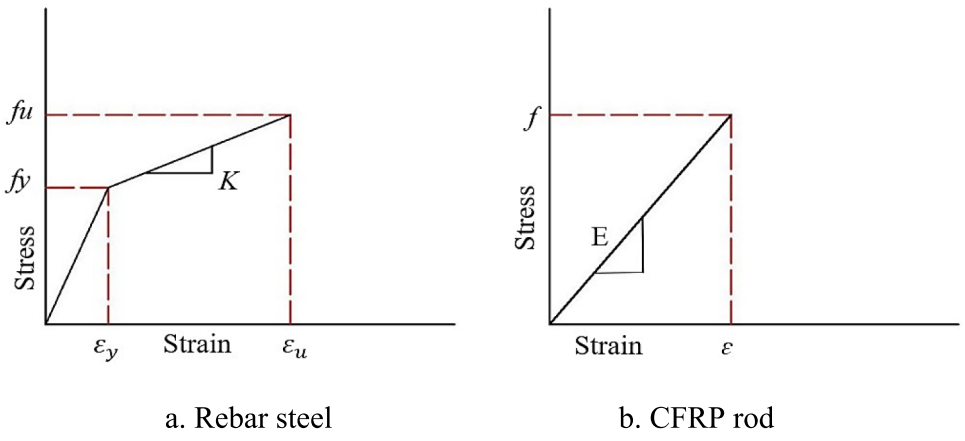

Fig. 9 Stress–strain relationship of steel and CFRP rod [43]

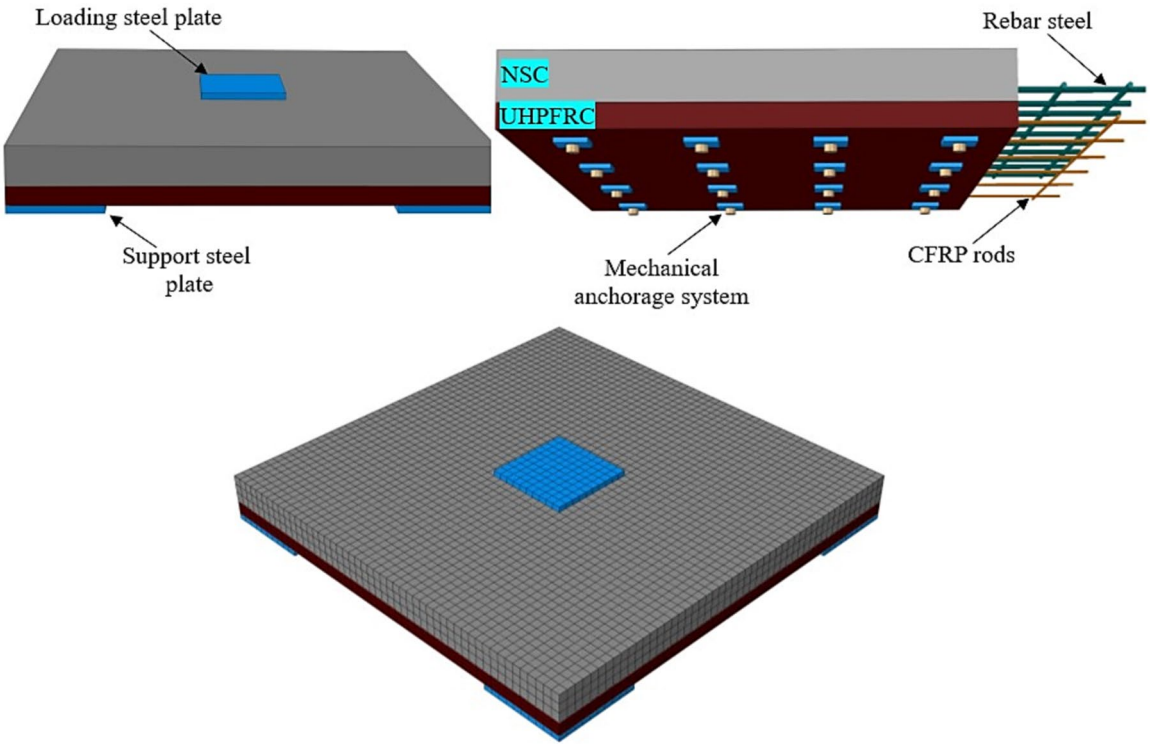

Fig. 10 Assembly and layout the strengthened slab

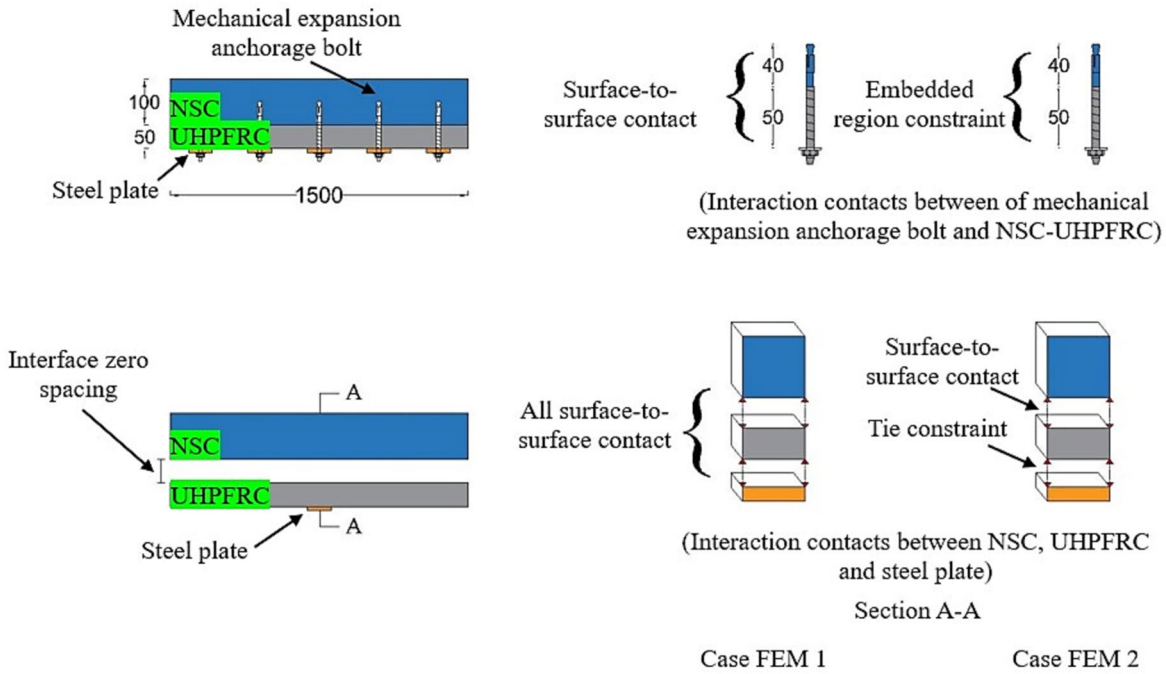

Fig. 11 Details of interaction contact models

4.4 Interaction contact models

In Abaqus software, the interaction connection between two different elements can be modeled using various techniques. Figure 11 displays all the interaction contact models used in the study. The perfect bonding "embedded region" contact

Table 5 Cases of the interaction contact modeling

Cases	Interface contact			
	B-N-U	*N-U*	*S-U*	*R-N & C-U*
FEM 1	Surface to surface			Embedded region
FEM 2	Embedded region	Surface to surface	Tie constraint	Embedded region

B-N-U; represents the interaction contact model between the expandable bolt and NC-UHPFRC, *N-U*; represents the contact model between NC-UHPFRC layers, *S-U*; represents the contact model between a steel plate and a UHPFRC layer, *R-N & C-U* represent the contact model between reinforcing steel bar and CFRP rod with NC and UHPFRC layers, respectively

approach was utilized to simulate the contact model between the CFRP bars and reinforcing steel with the UHPFRC and NC layers, respectively, as shown in Table 5. However, the contact between the UHPFRC and NC was defined as surface-to-surface and hard-contact in a normal direction, along with predefined friction coefficient [17], as displayed in Fig. 11. Additionally, two different contacts were used to simulate the interaction model between the expandable anchor bolt and NC and UHPFRC layers. The first was a surface-to-surface contact using hard-contact in a normal-direction along with a friction-coefficient (Fig. 11 Case FEM 1), and the second was an "embedded region" constraint (Fig. 11 Case FEM 2). The friction coefficient was considered [0.6] [17] at the contact between NC-UHPFRC, and [0.7] between the mechanical anchor system and NC-UHPFRC [40]. At the same time, two various interaction contact models between a steel plate and the underside face of a UHPFRC jacket were represented as a “surface-to-surface” (Case FEM 1) and "tie constraint" contact (Case FEM 2). Table 5 describes all cases of the interaction modeling contact that was used in the study.

5 Results and validation

5.1 Load–deflection behavior

Figure 12 illustrates the half–cyclic load versus displacement for experimental specimens. Table 6 demonstrates a comprehensive overview of the test results. The maximum load of the SB1 slab (benchmark slab) was 164kN, which improved to 264kN and 298kN in the (SB2, SB3) strengthened slab specimens, respectively. Notably, the slab specimen (SB2) increased the load capacity by 61%, while the slab (SB3) enhanced a slab by 82%, compared with benchmark slab, as indicated in Table 6. According to Fig. 12, strengthened specimens (SB2, SB3) showed a considerable improvement in the stiffness, specifically in the later phases of the elastic stage, compared with benchmark slab. The slope curve (load-deflection) for the reinforced slabs (SB3 and SB2) consistently exceeded that of the SB1 specimen during the whole testing duration, suggesting that the flexure

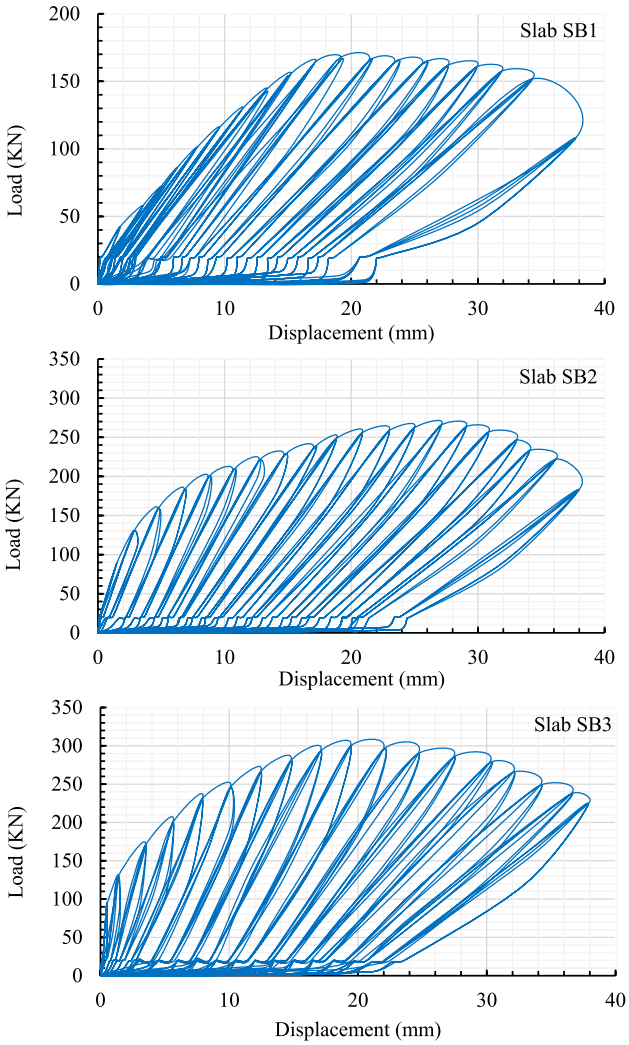

Fig. 12 Hysteretic half–cyclic load versus deflection for experimental specimens

stiffness was higher compared to the un-strengthened slab (SB1). In addition, this refers to the expansion of cracks on the tension side of the (SB1) specimen. However, for the reinforced SB3 slab specimen, the incorporation of CFRP mesh inside a UHPFRC layer led to a 13% enhancement in its load-bearing capability as compared with the SB2

Table 6 Summary results of experimental study

Slab	Pu (KN)	Δc (mm)	Δy (mm)	Δu (mm)	Increase in Pu (%)	Ductility (Δu/Δy)	Stiffness (kN/mm)
SB1	164	6.14	16	18	–	1.1	9.1
SB2	264	4.1	15	27	61	1.8	9.7
SB3	298	3.4	11	22.4	82	2.03	13.3

specimen. The results indicate that the CFRP rods effectively reduce deformations with improve the durability of the SB3 slab. The experimental findings offer valuable insights into future retrofitting techniques and the development of new materials and methods. Specifically, the application of UHPFRC in combination with steel plates and mechanical anchorage systems demonstrated promising results in terms of enhanced load-carrying capacity and improved ductility. These outcomes suggest that incorporating such materials into retrofitting designs could significantly extend the service life of reinforced concrete structures. By focusing on real-world applications, these findings contribute to shaping future retrofitting strategies that are both practical and robust. For the FE simulation, two various scenarios were used to simulate the interface contact between the expansion bolt and NC-UHPFRC layers, as mentioned before in Table 5. Table 7 presents the results of two cases of the FE simulation, along with their validation through experimental work. Figure 13 compares the cyclic load displacement of the FE specimens to the experimental slabs. The results demonstrated in Fig. 13 indicate a good agreement between FEM 1 and experimental outcomes. Compared to FEM 2, the specimens that adhered to the conceptual FEM1 displayed a greater similarity to the experimental study in terms of the load mid-span deflection curve. The maximum load of specimens in case FEM 2 increased from 279 and 329 kN to 260 kN and 312 kN for the FEM 1, respectively, as shown in Table 7. Nevertheless, the maximum load capacity of specimens FEM 1 exceeded that of the experimental slabs by roughly 3.12%, while FEM 2 models 8%. The variations in modeling strategies between FEM 1 and FEM 2 could clarify the differences in their performance when validated against experimental results. The used surface-to-surface interaction modeling between the NC-UHPFRC layers in FEM 1 is more realistic, accounting for possible slips or debonding between layers, while the assumed tie constraint between the layers in FEM 2, which may not capture the actual interaction during the analysis. The coefficient of variation (COV) values in Table 7 demonstrate the level of variability between the experimental and numerical results, with a lower COV indicating better consistency and alignment between the models and experimental data. In this study, the COV values of the FEM 1 models for both peak load and deflection were 0.036 and 0.051, respectively, while those for FEM 2 were slightly higher, at 0.052 and 0.057. The lower COV for FEM 1 suggests that it provides more reliable and consistent predictions compared to FEM 2. The higher COV for FEM 2 models indicates greater variability, potentially due to differences in the interactions modeled. These statistics further support the robustness of FEM 1 models in simulating the structural behavior of the slabs. On the other hand, these findings markedly enhance the understanding of the retrofitting method that uses CFRP and UHPFRC by illustrating the improved performance and reliability of FE models, particularly FEM 1, in mimicking actual structural behavior. This accuracy of results has practical ramifications for retrofitting methodologies, providing a verified approach for using CFRP and UHPFRC in the retrofitting approach, thereby advancing research focused on creating more resilient and durable retrofitting techniques

Table 7 Summary of two cases of the FE results

Cases	Slab ID	Pu (KN)	Δy (mm)	Δu (mm)	Ductility (Δu/Δy)	Stiffness (kN/mm)	Pu-f/Pu-e	Δu-f/Δu-e
FEM1	FEM 1-SB1	169	16.7	19.2	1.16	8.8	1.03	1.06
	FEM 1-SB2	260	13.8	26	1.88	10	0.98	0.96
	FEM 1-SB3	312	10.3	22	2.13	14.1	1.04	0.98
FEM2	FEM 2-SB2	279	15.2	28.1	1.85	9.93	1.06	1.04
	FEM 2-SB3	329	13.4	22.8	1.73	14.4	1.1	1.03
COV 1							0.036	0.051
COV 2							0.052	0.057

Pu-e and Δu-e represent the experimental peak load and deflection, as shown in Table 6, COV 1 and COV 2 represent the coefficient of variation between the experimental results and FE models in cases FEM 1 and FEM 2, respectively

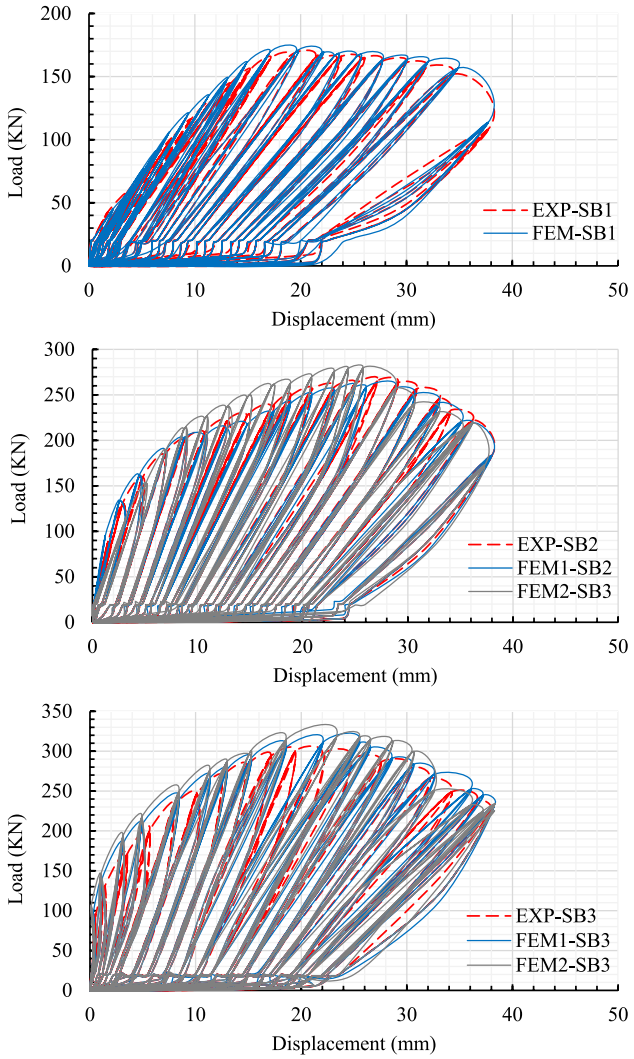

Fig. 13 Hysteretic half–cyclic load versus mid–span deflection of the FE and experimental slabs

essential for lengthening the lifespan of aging infrastructure and refining repair methodologies. Consequently, the link between the study's findings and their practical applications strengthens its overall contribution to the domain of structural retrofitting. In general, this leads to the conclusion that using the interface contact model between the expansion anchor bolt and NC-UHPFRC as designed in the first case, FEM 1, is more consistent with reality than the models in the second case, FEM 2, when compared to experimental results. Therefore, the results of case FEM 2 were neglected and not discussed in subsequent sections.

5.2 Failure behaviors and crack patterns

Figure 14 illustrates the failure mode observed during the experimental test. The SB1 slab experienced flexure failure behavior, resulting in a sudden and brittle failure. The load exhibited a linear increase, and the initial crack appeared at 79 kN, which corresponded to a deflection of 11 mm. Prior to the load reaching 130 kN, substantial lateral macrocracks were observed on the underside face of the SB1 slab. These cracks exhibited significant development and extended in various directions, as shown in Fig. 14a. Additionally, in the area of the applied load of the SB1 slab, a crushing concrete occurred. In contrast, the retrofitted (SB2, and SB3) slabs showed a different type of failure behavior from the SB1 slab. The cracking resistance of slabs SB2 and SB3 improved significantly, leading to a more linear stiffness response. As increased the load, (SB2, and SB3) slab specimens exhibited improved rigidity until reached cracking phases at 130kN and 156kN, respectively. Incorporation of CFRP rods inside the jacket of UHPFRC for the retrofitted (SB3) slab significantly contributed to strengthening the slab's tension zone and postponing the appearance of diagonal cracks, as shown in Fig. 14c. The failure occurred in the retrofitted SB3 slab when four cracks formed in opposing trends and appeared on the underside of the UHPFRC layer and beside the mechanical systems. Figure 15 displays the failure of the FE model next to the experimental failure for the purpose of additional validation and comparison. As illustrates in Fig. 15, the FE models demonstrated good agreement with the experiment outcomes in the patterns of flexural damage and cracks propagation. The failure occurred in the FE slabs (SB1, SB2, and SB3) when the ultimate load achieved to 169kN, 260kN, and 312kN, respectively, as illustrates in Table 7. The overall peak load of the FE specimens increased by 2.07% compared to the experimental results. Throughout the testing process, there were no instances of premature de -bonding between the NC-UHPFRC layers in the experimental study and FE simulations. Additionally, the mechanical expandable anchor bolts were not pulled of the specimens, as illustrates in Fig. 15b and c. This is primarily due to the high efficiency and effectiveness of the new suggested strengthening method. The plastic strain was more articulated in the underside face of the FEM specimens (SB2, SB3) than on the edges, as displayed in Fig. 15b and c. This demonstrates that a larger tensile-strain emerged in the center section of a UHPFRC jacket.

5.3 Ductility and elastic stiffness

Ductility refers to the concrete member's capacity to resist plastic deformation with beyond its yield point without fracturing. This study examined the ductility of the slabs by compressing the (SB1) to the retrofitted (SB2, SB3) slab specimens. Equation 11 was used to calculate the ductility indexes $[\mu\Delta u]$ according to the yield and maximum deflection [44].

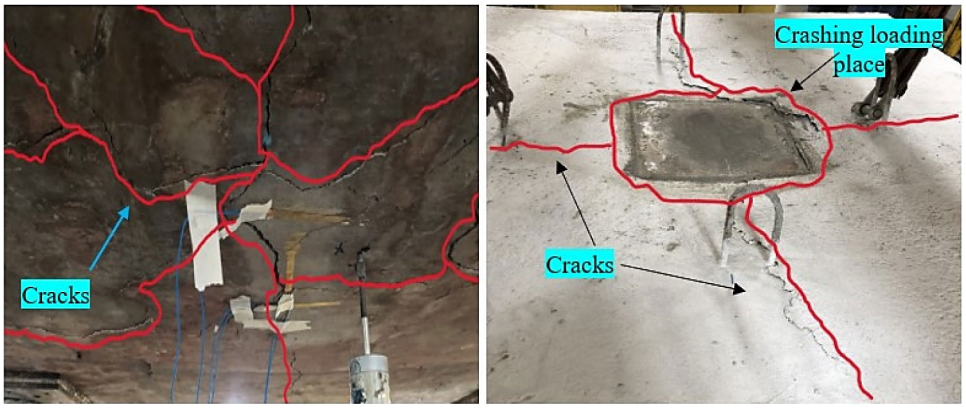

(a) SB2 slab

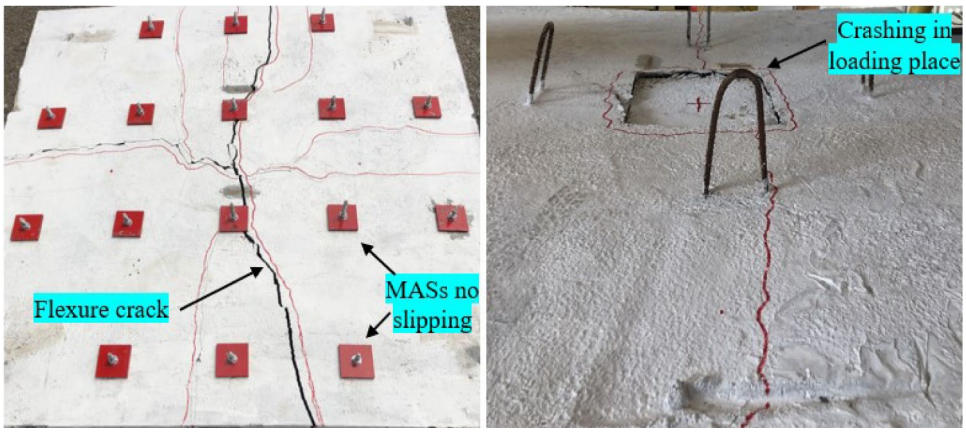

(b) SB2 slab

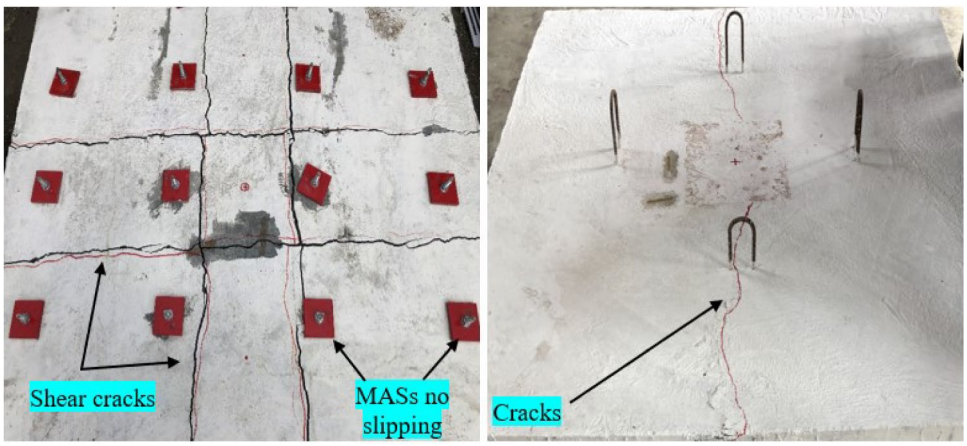

(c) SB3 slab

Fig. 14 Failure behavior crack pattern in top and bottom sides of experimental slabs

$$\mu\Delta u = \Delta u/\Delta y \tag{11}$$

Based on the results in Table 6, the ductility of retrofitted slabs (SB2, and SB3) is higher compared with control specimen. The ductility of the experimental specimens (SB1, SB2, and SB3) was 1.1, 1.8 and 2.03, respectively, as shown in Table 6. Additionally, the ductility of the finite element (FE) specimens was slightly greater compared to the experimental slabs. However, the ductility of the FE specimens achieved 2.18% at maximum load. Elastic stiffness, on the other hand, is characterized as linear portion of the maximum load mid-span displacement. However, the stiffness of

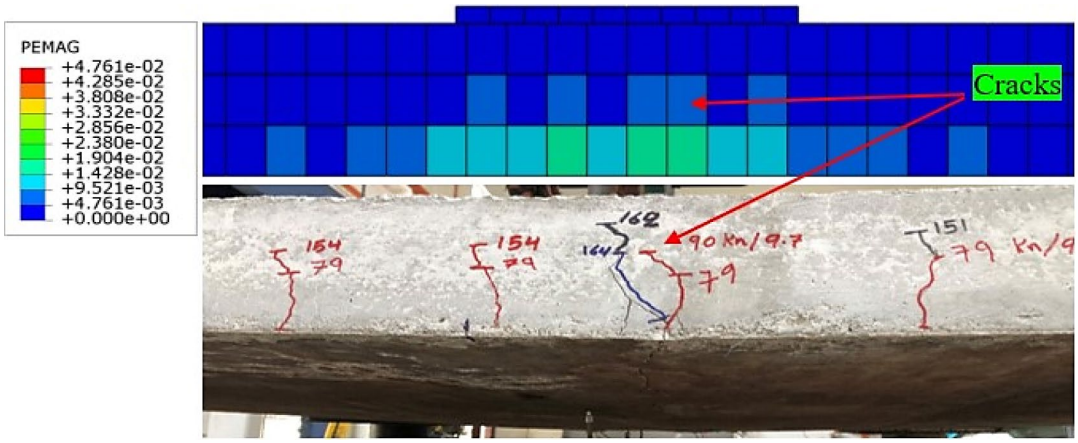

(a) SB1 slab

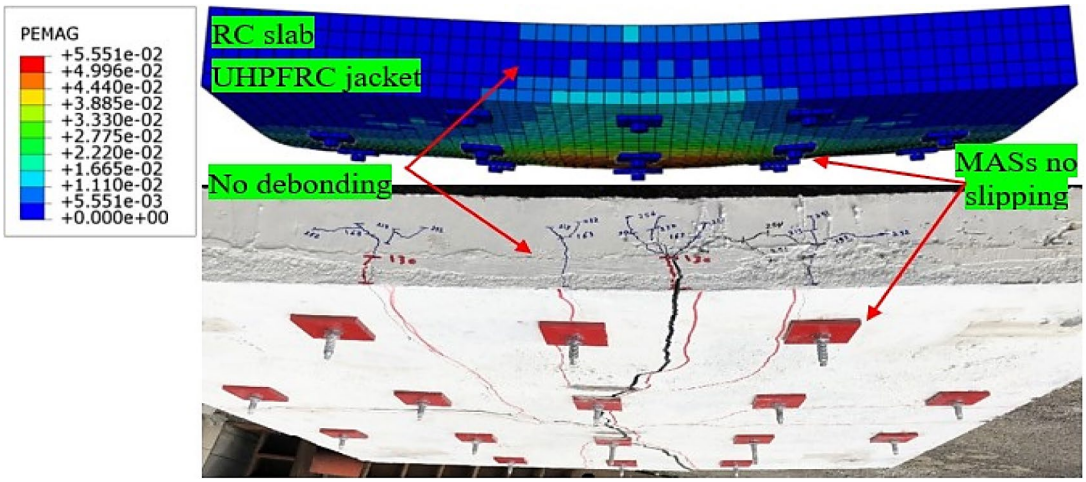

(b) SB2 slab

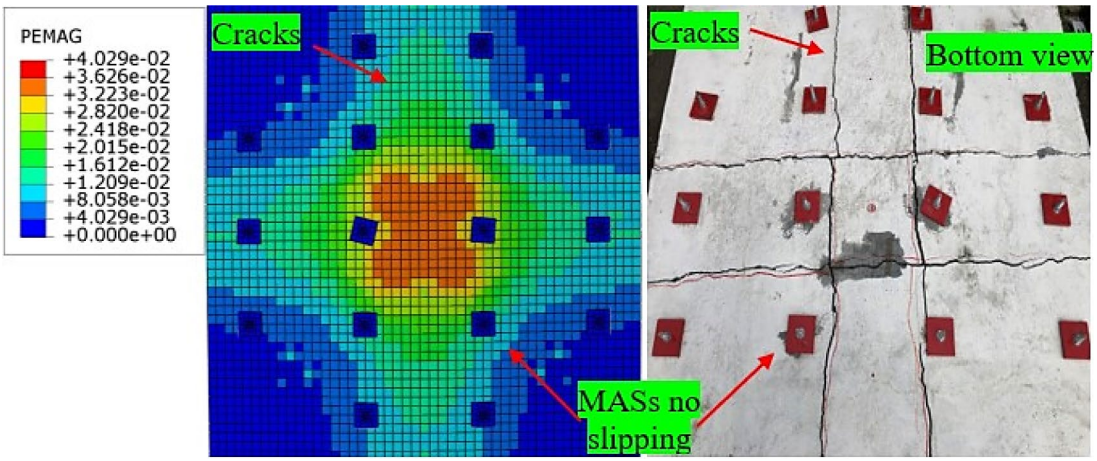

(c) SB3 slab

Fig. 15 Validation between the EF models and experimental slabs

retrofitted slabs (SB2, SB3) was 9.7kN/mm and 13.3kN/mm, respectively, whereas the control specimen (SB1) showed a stiffness of 9.1kN/mm, as depicted in Table 6. In addition, the FE models' stiffness increased by 4.91%, compared to the experimental slabs. Based on the experimental outcomes, a new retrofitting method has significantly enhanced the ductility of the strengthened specimens (SB2, SB3) compared with benchmark slab (SB1). Furthermore, the EF results for ductility and elastic stiffness nearly match the experimental results, indicating a good agreement between the FE models and the experimental outcomes.

5.4 Strain response of CFRP rods and reinforcing steel

Table 8 depicts the maximum strain in rebar steel and CFRP bars determined by experimental and FE results. The strain in both CFRP rods and reinforcing steel was specified by obtaining the average maximum strain values of the four rebars located in the midpoint and opposite directions. Figure 16 illustrates the load–strain relationships for the reinforcement steel and CFRP bars in both the numerical and experimental. The ultimate strain of rebar steel inside the NC of the retrofitted specimens (SB2, SB3) was notably smaller than that of control specimen. The reduction in maximum strain noticed in the retrofitted SB2, and SB3 slabs indicates that the load bearing capacity and resistance to deformation of the slabs have been enhanced due to the bonding of an exterior UHPFRC jacket. The rebar steel in the SB3 slab exhibited a peak strain of 0.002485 mm, which was significantly less compared with specimens (SB1, and SB2), as indicated in Table 8. This drop in tensile stress is related to the incorporation of GFRP bars inside the UHPFRC jacket that increases the tensile capacity of rebar steel. In contrast, the FEM models exhibited a good level of agreement with the practical work in terms of ultimate strain in rebar and CFRP rods, as shown in Fig. 16. The differences between the maximum strain of reinforcement steel and CFRP bars from the FEM simulation and the experimental test were generally smaller than 7.6% and 5.75%, respectively, as depicted in Table 8. This demonstrates that the finite-element models exhibit a high level of accuracy in predicting the response of strain in the CFRP bars and rebar steel.

5.5 Parametric study

After verifying the FEM's ability to expect the response of a retrofitted slab employing CFRP bars with a UHPFRC layer and mechanical anchor systems, parametric study was performed to examine the impact of various parameters

Table 8 Maximum strain in steel and CFRP bars for experimental and FEM models

ID	EXP		FEM		Difference	
	Rebar s (%)	CFRP bars (%)	Rebar-F (%)	CFRP-F (%)	Rebar s (%)	CFRP bars %
SB1 slab	0.3474	–	0.3793	–	9.18	–
SB2 slab	0.3006	–	0.3202	–	6.52	–
SB3 slab	0.2485	0.3755	0.2657	0.3971	6.92	5.75

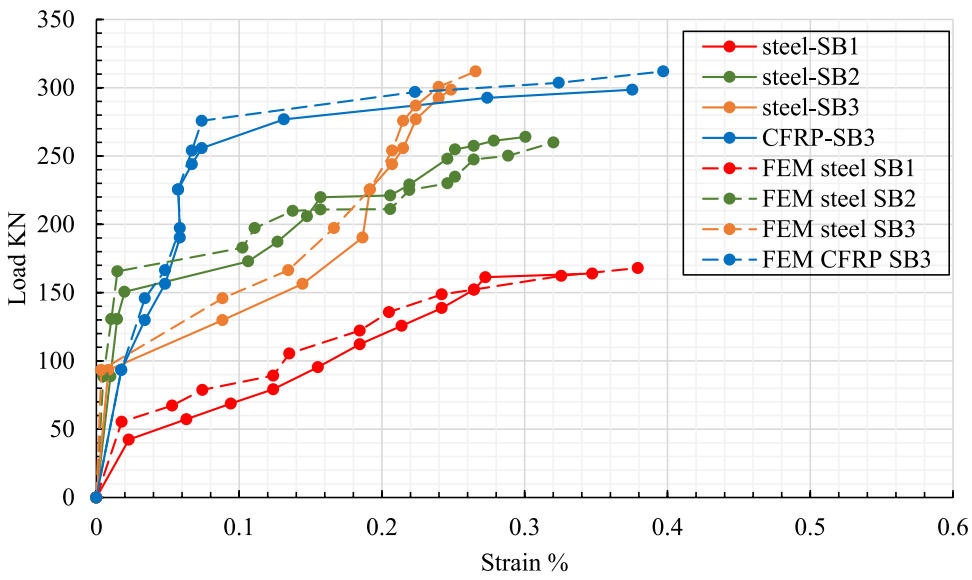

Fig. 16 Load–strain relationship of steel and CFRP bars for experimental and FE models

Table 9 Parameters of the parametric investigations

Group	ID models	Variable
Group–1	SB2-BD10	Bolt diameter (D10)
	SB2-BD14	Bolt diameter (D14)
	SB2-BD16	Bolt diameter (D16)
	SB3-BD10	Bolt diameter (D10)
	SB3-BD14	Bolt diameter (D14)
	SB3-BD16	Bolt diameter (D16)
Group–2	SB2-NJ50	Normal strength concrete jacket (C 50)
	SB2-NJ80	Normal strength concrete jacket (C 80)
	SB3-NJ50	Normal strength concrete jacket (C 50)
	SB3-NJ80	Normal strength concrete jacket (C 80)
Group–3	SB2-CS	Proposed system in a compressive side
	SB3-CS	Proposed system in a compressive side
Group–4	SB3-RD8	Rebar and diameter in UHPFRC jacket (8 mm)
	SB3-RD10	Rebar and diameter in UHPFRC jacket (10 mm)
	SB3-RD12	Rebar and diameter in UHPFRC jacket (12 mm)

that could potentially influence the behavior of RC slabs. Four series of retrofitted slabs with different parameters were designed. Table 9 depicts the study's major parameters, which include the diameter of mechanical expansion anchorage bolts, a normal strength concrete (NSC) jacket with various grades of concrete rather than the UHPFRC jacket, applying the proposed retrofitting system on a compressive side instead of a tension zone as in the experimental study, and, finally, using reinforcing steel bars of varying diameters inside the UHPFRC layer instead of CFRP bars. Table 10 demonstrates the parametric study outcomes.

$$D1 = \frac{\text{Ultimate load of FE models}}{\text{Ultimate load of experimental}};$$

$$D2 = \frac{\text{Deflection at an ultimate load of FE models}}{\text{Deflection at an ultimate load of experimental}}$$

5.5.1 Effect of mechanical expansion anchorage bolt diameter

The influence of the diameters of mechanical expansion anchor bolts for the retrofitted slabs was evaluated using six different FE models, as shown in Table 9. The present investigation used mechanical expansion anchorage bolts with diameter sizes of (10, 14, and 16) mm, as illustrated in Table 9, and compared to the experimental work that used anchor bolts 12 mm in diameter. Figure 17 depicts the load–deflection curve of both the experimental specimens and FE models with different diameters of mechanical anchor bolts. Compared to the experimental work, the peak load of the SB2-BD10, and SB3-BD10 specimens, which used a 10 mm diameter of the expandable anchor bolts, decreased from 264 and 298kN to 253kN and 282kN, respectively. The models that used 14 mm and 16 mm diameters of mechanical expansion anchorage bolts increased the maximum load by 8%, and 12%, respectively. The study concluded that the use of mechanical expandable anchor bolt with a diameter larger than 12 mm significantly enhanced the performance of slabs.

Table 10 Summary of the parametric study results

Group	Slab ID	Pu (KN)	Δu (mm)	D1	D2	Stiffness (KN/mm)
Group–1	SB2-BD10	253	28.2	0.95	1.04	8.97
	SB2-BD14	271	27.3	1.02	1.01	9.93
	SB2-BD16	277	27.7	1.04	1.02	10
	SB3-BD10	282	24.4	0.95	1.09	11.55
	SB3-BD14	314	23.7	1.05	1.06	13.25
	SB3-BD16	326	23.1	1.09	1.03	14.1
Group–2	SB2-NJ50	191	32	0.72	1.18	5.9
	SB2-NJ80	198	30.6	0.75	1.13	6.5
	SB3-NJ50	228	28.3	0.76	1.27	8
	SB3-NJ80	236	27.6	0.79	1.23	8.55
Group–3	SB2-CS	223	28	0.84	1.04	7.96
	SB3-CS	263	24.8	0.88	1.11	10.6
Group–4	SB3-RD8	227	26	0.76	1.16	8.73
	SB3-RD10	239	25.1	0.8	1.12	9.52
	SB3-RD12	257	24.3	0.86	1.08	10.57

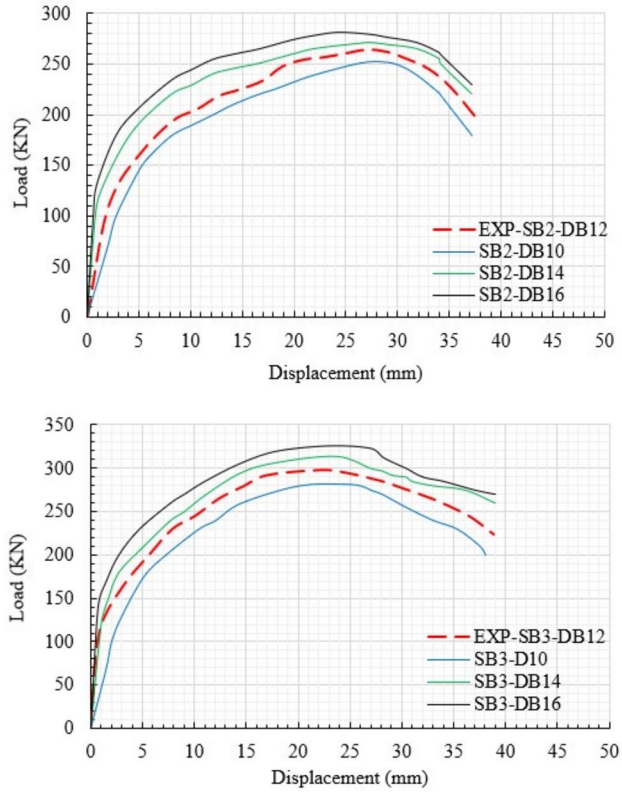

Fig. 17 Load versus deflection curves of models with different mechanical expansion anchor bolt diameters

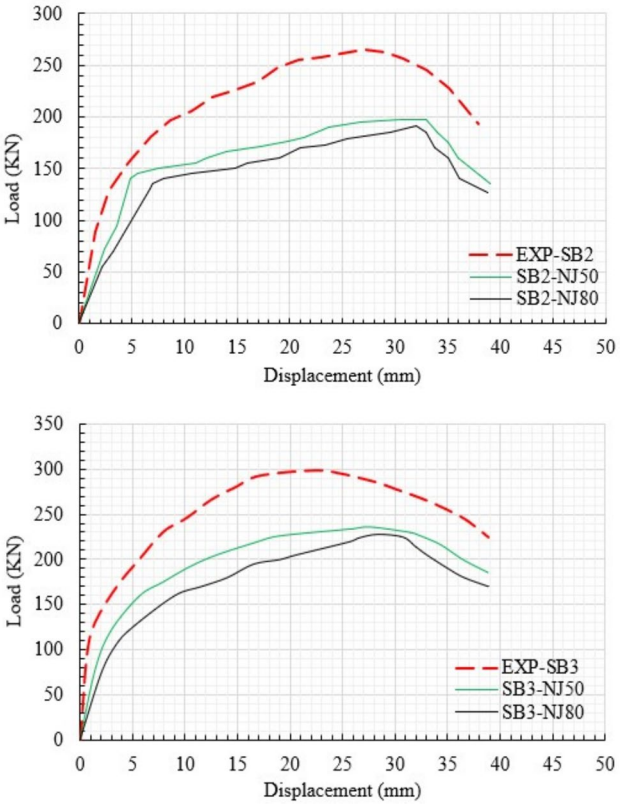

Fig. 18 Load–displacement curves for FE models with NSC jacket and various grades of concrete

5.5.2 Effect of used NSC jacket and grades of concrete

Figure 18 illustrates the impact of concrete jacketing and concrete grades on the overall effectiveness of the retrofitted slabs. Four models were designed using NSC jackets with grades of C50 and C80 instead of UHPFRC jacketing. Based on Table 10, the SB2-NJ models utilized NSC jackets and had differing concrete grades ranging from 50 to 80MPa. The variation in peak load of the SB2-NJ models was 73 kN and 80 kN, respectively, compared to the experimental slabs. Contrary, the maximum load differences for SB3-NJ were 70kN and 62kN, respectively. However, the deflections of all FE models increased compared to the experimental specimens, resulting in a decrease in their overall stiffness. Overall, in the suggested strengthening method, the use of NC jackets with grades C50 and C80 significantly impacted slab performance.

5.5.3 Applying proposed strengthening system in a compressive side

Two finite-element specimens were created to assess the impact of the applying suggested strengthening method in the compressive side, as depicts in Fig. 19 and Table 9. Figure 20 shows the load–displacement relationship of slabs retrofitted in the compressive side using the newly proposed system. According to Table 10, the maximum load capacity of the slabs was affected by the implementation of the new suggested retrofitting method in the compressive side of the slab. The ultimate load of SB2-CS and SB3-CS models reduced by 14% and 12%, respectively, compared to the experimental specimens (SB2, SB3). In addition, the stiffness of the models reduced from 9.7kN/mm and 13.3kN/mm to 7.96kN/mm and 10.6kN/mm, respectively. This is primarily due to the failure behavior of SB2-CS and SB3-CS slabs was not controlled by NSC tension capacity or reinforcing steel in the slabs. Thus, it can be inferred that using a proposed strengthening system on the compression side of the slab significantly impacts the performance of the slab.

5.5.4 Effect of steel rebar and diameter

The effect of using reinforcing steel bars with different diameters rather than CFRP rods in the UHPFRC jacket on the suggested strengthening system was evaluated employing rebar steel diameters of (8, 10, and 12) mm, as illustrated in Table 9. Figure 21 demonstrates the load–deflection curves of the finite-element models using reinforcement steel in

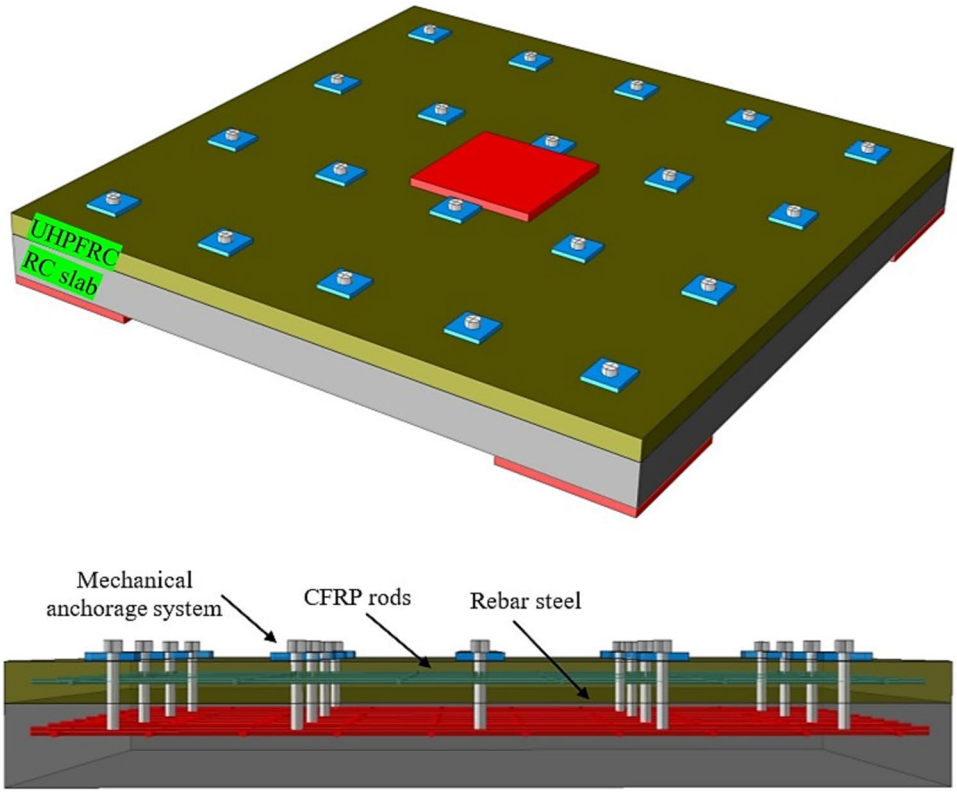

Fig. 19 Scheme of strengthening RC slab in the compressive side

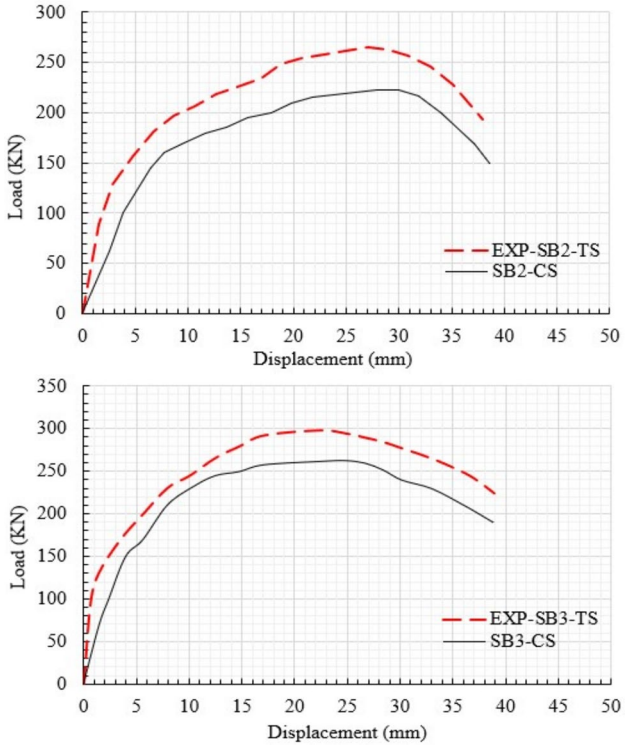

Fig. 20 Load–displacement relationship of models retrofitted on the compressive side

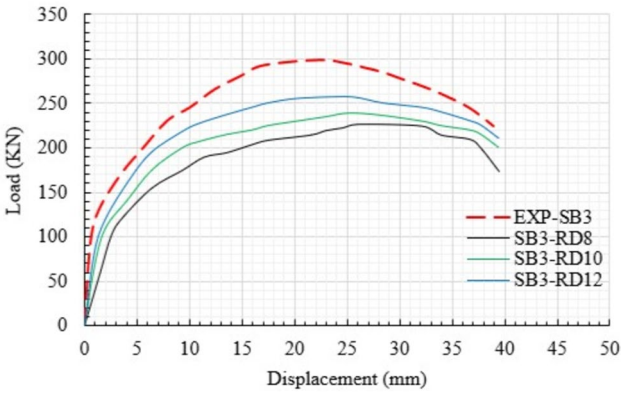

Fig. 21 Load–displacement curves of models with various steel bar diameters

the UHPFRC jacket with different diameters. In the model SB3-RD8 with reinforcing steel bar diameters of 8 mm, the ultimate load decreased from 298 to 272kN, and mid-span deflection increased from 22 to 25 mm. However, for the SB3-RD10 and SB3-RD12 slab models, increasing the diameter of the rebar steel from 8 to 10 mm and 12 mm resulted in an increase in the slab's carrying capacity by approximately 11% and 14.7%, respectively, compared to the SB3-R8 model. The use of reinforcing steel bars instead of CFRP rods in this proposed strengthening system reduced

the overall ultimate load by 8% compared to the experimental study. In general, these findings suggest that the use of reinforcing steel bars with increasing cross-sectional area has a significant adverse impact on the proposed retrofitting system.

6 Comparison with other techniques

The utilization of expandable bolts as mechanical anchor systems in the suggested retrofitting technique has numerous benefits compared to alternative prevalent anchoring strategies, such as adhesive bonding or dowel anchoring, especially regarding efficacy and ease of implementation. Expanding bolts are highly effective in establishing robust mechanical interlocking between the slab and new UHPFRC. This method efficiently handles the problem of debonding, a prevalent concern in retrofitting applications, thereby improving load transfer and augmenting the structural integrity of the composite system. Conversely, adhesive-based anchors, like epoxy-bonded CFRP laminates, frequently exhibit vulnerability to bond breakdown due to cyclic loads, temperature fluctuations, or moisture exposure. Dowel bars, although mechanically efficient, may lack consistent bonding and could be susceptible to movement or alignment problems if not put with precision. As for the implementation aspect, expansion bolts are simple to install, necessitating only ordinary drilling and tightening procedures that are uncomplicated and do not require prolonged curing time or specialized tools. In contrast to adhesive anchors, which require meticulous surface preparation, accurate mixing, and curing duration, expansion bolts can be swiftly fitted and loaded, hence minimizing construction time. Dowel anchoring entails drilling holes for rebar insertion and frequently necessitates intricate grouting processes to stabilize the rebar within the existing concrete. This may require more labor and time than the installation of expansion bolts. General, expansion bolts provide a pragmatic equilibrium between ease of application and durability, making them especially beneficial for retrofitting endeavors that emphasize long-term performance while seeking to reduce installation complexity. On the other hand, according to Sect. 1, the proposed retrofitting technique provides good resistance to various environmental conditions such as corrosion, fire, and freeze–thaw due to the UHPFRC's high-density composition and low porosity compared to conventional concrete. By preventing the possibility of premature debonding, this system can contribute to the longer-term durability of slabs, minimizing the necessity for regular repairs or maintenance. This significantly impacts the reduction of long-term maintenance costs and improves the overall durability of retrofitted slabs, making it a highly practical advancement in the field of structural retrofitting. On the other hand, the results of this study provide significant insights that may be applicable to different retrofitting materials and techniques, particularly regarding bonding issues and structural integrity under cyclic loads. The proven efficacy of the mechanical anchorage system in preventing premature debonding and enhancing load transfer indicates that this method may enhance retrofitting techniques utilizing materials with comparable bonding challenges, including fiber-reinforced polymers (FRPs), even in retrofits that involve bonding steel plates or metal reinforcements to concrete structures, or alternative concrete overlays. Nevertheless, the generalization to materials must be undertaken with caution, as various retrofitting materials exhibit various mechanical properties, bonding properties, and stress responses. Further research and experimental verification are required to refine the anchorage design and modify parameters to suit the specific requirements of materials or retrofitting scenarios.

7 Economic feasibility of retrofitting system

The economic feasibility of the proposed retrofitting technique can be evaluated by examining the costs of each component. All prices of materials used are according to the Malaysian market UHPFRC, which costs 2200–2400$ per cubic meter, and its design quantity used in the system is 285 kg/m3. The total cost of UHPFRC is 684$. 18m length of CFRP rods contributes $122.5 to the cost, while 20 anchor bolts and steel plates add $60.2 and $55.2, respectively. Therefore, the cost of the proposed retrofitting technique is 921.9 $. Notably, this cost excludes any supplementary implementation fees as the study was conducted in the laboratories of the university. In comparison to the conventional retrofitting techniques, such as FRP laminates or steel reinforcement, the suggested approach may initially seem more expensive. Conventional solutions frequently utilize less expensive materials, such as normal concrete, steel reinforcement bars, or adhesive-bonded FRP sheets, leading to reduced initial expenses. Nevertheless, conventional methods are generally more subject to debonding and degradation under cyclic loading and environmental conditions, which may result in repeated repairs and heightened maintenance costs over time. The proposed method, featuring greater bonding between jacket and slab, eliminates the possibility of premature debonding and provides increased durability, particularly under cyclic loads. This may result in reduced long-term maintenance expenses and prolong the structure's lifespan, relative to the conventional approaches, hence mitigating the elevated initial cost of the proposed system.

8 Conclusion

This study investigates the experimental and numerical aspects of enhancing RC slabs by mechanically anchoring system an external UHPFRC jacket to the tensile surface of slabs. Consequently, the experimental tests were achieved on the slabs using the newly suggested retrofitting system by applying incremental repeating loads (cyclic loads). The finite element simulation outcomes have been validated with the experimental results. In addition, a parametric study was conducted to determine the impact of various parameters on the performance of RC slabs employing CFRP bars and an external UHPFRC jacket. Based on the results, the following conclusions can be drawn:

- The new proposed strengthening technique significantly improved the resistance of initial cracks. SB2 and SB3 strengthened slabs experienced 82% increased initial cracking loads.
- The peak load capacity of retrofitted slabs increased, with specimens (SB2, SB3) experiencing an improvement in maximum loads by 61% and 82%, respectively.
- In the (SB3) slab, the incorporating of CFRP mesh inside the jacket of UHPFRC resulted in a notable 13% increase of the slab's maximum load, compared with SB2.
- The proposed strengthening technique eliminated the case of early de-bonding. No de-bonding emerged between the NC and UHPFRC layers during all stages of the test. Remarkably, the mechanical anchor systems remained securely in place within the slabs until the failure phase. By preventing the possibility of premature debonding, this system can contribute to the longer term durability of slabs, minimizing the necessity for regular repairs or maintenance. This significantly impacts the reduction of long-term maintenance costs and improves the overall durability of retrofitted slabs, making it a highly practical advancement in the field of structural retrofitting.
- The developed finite-element models (FEM) for non-composite and composite demonstrated a good level of concurrence with experimental outcomes.
- Representing the surface-to-surface interface contact model between the expandable bolt and NC-UHPFRC showed more accuracy in the results than using the embedded region constraint technique.
- In the models that followed case FEM 1, the coefficient of variation (COV) between the experimental and FE specimens in terms of maximum loads and mid-span displacements were 0.036, and 0.051, respectively, whereas the models in case FEM 2 were 0.052 and 0.057. These reduced variabilities of the results in the FEM 1 models suggest a strong alignment between the model's predictions and the experimental data, supporting the robustness of the proposed technique and its potential for real-world applications.
- Increasing a cross–sectional area of the mechanical expansion anchorage bolts improved the peak load by 10%.
- The use of NSC jackets with grades C50 and C80 instead of a UHPFRC jacket in the proposed retrofitting system reduced the overall stiffness of the slabs by 48.61%.
- Applying the new proposed strengthening system on the compressive side reduced the ultimate load of slabs overall by 13%.
- The adoption of reinforcing steel bars rather than CFRP rods in the UHPFRC jacket resulted in an 8% reduction in overall ultimate load.

From the parametric study, the results could inform the design recommendations or retrofitting practices by highlighting the significance of choosing the appropriate materials such as jacket material and cross–sectional area of anchor bolt to optimize load distribution and structural integrity. Besides, these insights could shape future retrofitting techniques by guiding engineers in material selection and anchorage design to improve the performance of retrofitted structures, potentially leading to more efficient, cost-effective, and safer retrofitting solutions in the field. The current study demonstrated the importance of considering the interactions between the expansion anchor bolt and NC-UHPFRC in the FE analysis of composite concrete members. To enhance the predictive accuracy of the finite-element models with complex interactions, it is essential to consider bond slip behavior between the NSC and the UHPFRC or nonlinear material properties under various loading circumstances. Nevertheless, in future studies, a combination of two strengthening technologies to improve slab shear and flexural performance, further parameters to design the RC slab's properties, such as geometric slab, and reinforcing steel bar ratio, should be examined.

Declarations

Conflict of interest It is declared that there is no conflict of interest in this research work.

Ethical approval There are no ethical concerns in this research work.

References

1. Le Hoang A, Fehling E. Influence of steel fiber content and aspect ratio on the uniaxial tensile and compressive behavior of ultra high performance concrete. Constr Build Mater. 2017;153:790–806. https://doi.org/10.1016/j.conbuildmat.2017.07.130.
2. Tayeh BA, Bakar BA, Johari MM, Voo YL. Mechanical and permeability properties of the interface between normal concrete substrate and ultra high performance fiber concrete overlay. Constr build mater. 2012;36:538–48. https://doi.org/10.1016/j.conbuildmat.2012.06.013.
3. Brühwiler E, Denarié E. Rehabilitation and strengthening of concrete structures using ultra-high performance fibre reinforced concrete. Struct Eng Int. 2013;23(4):450–7. https://doi.org/10.2749/101686613X13627347100437.
4. Wu Z, Shi C, Khayat KH. Investigation of mechanical properties and shrinkage of ultra-high performance concrete: Influence of steel fiber content and shape. Compos Part B: Eng. 2019;174:107021. https://doi.org/10.1016/j.compositesb.2019.107021.
5. Noshiravani T, Brühwiler E. Rotation capacity and stress redistribution ability of R-UHPFRC-RC composite continuous beams: an experimental investigation. Mater Struct Constr. 2013;46(12):2013–28. https://doi.org/10.1617/s11527-013-0033-5.
6. Habel K, Gauvreau P. Response of ultra-high performance fiber reinforced concrete (UHPFRC) to impact and static loading. Cem Concr Compos. 2008;30(10):938–46. https://doi.org/10.1016/j.cemconcomp.2008.09.001.
7. Chun B, Yoo DY. Hybrid effect of macro and micro steel fibers on the pullout and tensile behaviors of ultra-high-performance concrete. Compos Part B: Eng. 2019;162:344–60. https://doi.org/10.1016/j.compositesb.2018.11.026.
8. Murthy AR, Karihaloo BL, Rani PV, Priya DS. Fatigue behaviour of damaged RC beams strengthened with ultra high performance fibre reinforced concrete. Int J Fatigue. 2018;116:659–68. https://doi.org/10.1016/j.ijfatigue.2018.06.046.
9. El-Mandouh MA, Elsamak G, Rageh BO, Hamoda A, Abdelazeem F. Experimental and numerical investigation of one-way reinforced concrete slabs using various strengthening systems. Case Stud Constr Mater. 2023;18:e01691. https://doi.org/10.1016/j.cscm.2022.e01691.
10. Nadir W, Kadhimi MMA, Jawdhari A, Fam A, Majdi A. RC beams strengthened in shear with FRP-Reinforced UHPC overlay: an experimental and numerical study. Structures. 2023;53(April):693–715. https://doi.org/10.1016/j.istruc.2023.04.117.
11. Wang H, Zhou Z, Zhang Z, Zou Y, Jiang J, Zeng X. Experimental and numerical studies on shear behavior of prefabricated bridge deck slabs with compact UHPC wet joint. Case Stud Const Mat. 2023;19:e02362. https://doi.org/10.1016/j.cscm.2023.e02362.
12. Su YL, Wu C, Shang JQ, Zhang P, Sheikh SA. Experimental and numerical simulation research on the flexural performance of beams reinforced with GFRP bars and three-sides UHPC layer. Structures. 2024;59:105746. https://doi.org/10.1016/j.istruc.2023.105746.
13. Shan Y, et al. Flexural behavior of ultra-high performance concrete (UHPC) shaped thin-plate ribbed staircases: an experimental and numerical study. Mater Struct Constr. 2024;57(1):1–17. https://doi.org/10.1617/s11527-023-02282-x.
14. Safdar M, Matsumoto T, Kakuma K. Flexural behavior of reinforced concrete beams repaired with ultra-high performance fiber reinforced concrete (UHPFRC). Compos Struct. 2016;157:448–60. https://doi.org/10.1016/j.compstruct.2016.09.010.
15. Paschalis SA, Lampropoulos AP, Tsioulou O. Experimental and numerical study of the performance of ultra high performance fiber reinforced concrete for the flexural strengthening of full scale reinforced concrete members. Constr Build Mater. 2018;186:351–66. https://doi.org/10.1016/j.conbuildmat.2018.07.123.
16. Ramachandra Murthy A, Karihaloo BL, Priya DS. Flexural behavior of RC beams retrofitted with ultra-high strength concrete. Constr Build Mater. 2018;175:815–24. https://doi.org/10.1016/j.conbuildmat.2018.04.174.
17. Ahmed S, Mohamed EY, Mohamed HA, Emara M. Experimental and numerical investigation of flexural behavior of RC beams retrofitted with reinforced UHPFRC layer in tension surface. Structures. 2023;49:106–23. https://doi.org/10.1016/j.istruc.2023.01.113.
18. Al-Osta MA, Isa MN, Baluch MH, Rahman MK. Flexural behavior of reinforced concrete beams strengthened with ultra-high performance fiber reinforced concrete. Constr Build Mater. 2017;134:279–96. https://doi.org/10.1016/j.conbuildmat.2016.12.094.
19. Li C, Aoude H. Influence of UHPFRC jacketing on the static, blast and post-blast behaviour of doubly-reinforced concrete beams. Int J Impact Eng. 2023;179:104656. https://doi.org/10.1016/j.ijimpeng.2023.104656.
20. Yang J, Yu J, Zhang Z, Zou Y, Chen R, Zhou J, Li B. Flexural behavior of 15-year-old full-scale hollow slab beams strengthened with fiber-reinforced composites. Case Stud Constr Mater. 2023;19:e02545. https://doi.org/10.1016/j.cscm.2023.e02545.
21. Sun W, Fan W, Yang J, Wu Q, Zhong Z. Numerical simulation and design method of the interface of UHPFRC-strengthened RC structures using post-installed rebars. Eng Struct. 2023;15(289):116286. https://doi.org/10.1016/j.engstruct.2023.116286.
22. Saeed FH, Hejazi F, Rashid RS. Strengthening of reinforced concrete slabs using carbon fiber reinforced polymers rods and concrete jacket with a mechanical anchorage system. Constr Build Mater. 2024;440:137464. https://doi.org/10.1016/j.conbuildmat.2024.137464.
23. Hong SG, Lim WY. Strengthening of shear-dominant reinforced concrete beams with ultra-high-performance concrete jacketing. Constr Build Mater. 2023;365:130043. https://doi.org/10.1016/j.conbuildmat.2022.130043.
24. Paschalis SA, Lampropoulos AP. Developments in the use of ultra high performance fiber reinforced concrete as strengthening material. Eng Struct. 2021;233:111914. https://doi.org/10.1016/j.engstruct.2021.111914.
25. Said A, Elsayed M, Abd El-Azim A, Althoey F, Tayeh BA. Using ultra-high performance fiber reinforced concrete in improvement shear strength of reinforced concrete beams. Case Stud Constr Mater. 2022;16:e01009. https://doi.org/10.1016/j.cscm.2022.e01009.
26. Mostofinejad D, Moghaddas A. Bond efficiency of EBR and EBROG methods in different flexural failure mechanisms of FRP strengthened RC beams. Constr Build Mater. 2014;54:605–14. https://doi.org/10.1016/j.conbuildmat.2014.01.002.
27. Coelho MRF, Sena-Cruz JM, Neves LAC. A review on the bond behavior of FRP NSM systems in concrete. Constr Build Mater.

2015;93:1157–69. https://doi.org/10.1016/j.conbuildmat.2015.05.010.
28. T. Datasheet, "Hilti Hst3 Expansion Anchor."
29. I. Units, 318–19 Building Code Requirements for Structural Concrete and Commentary. 2019.
30. Pedram Z, Xiong Y, Xin J, Amir M. Punching shear enhancement of flat slabs with partial use of ultrahigh-performance concrete. J Mater Civ Eng. 2015;27(9):4014255. https://doi.org/10.1061/(ASCE)MT.1943-5533.0001219.
31. Bars S, et al. Standard specification for general requirements for steel bars, carbon and alloy, hot-wrought 1 title of specification ASTM designation A. Constr Build Mater. 2013;1:1–16. https://doi.org/10.1520/A0029.
32. Zhang Y, Wang H, Qin Y, Huang S, Fan W. Experimental and analytical studies on the flexural behavior of steel plate-UHPC composite strengthened RC beams. Eng Struct. 2023;283:115834. https://doi.org/10.1016/j.engstruct.2023.115834.
33. A. C. I. C. 239, ACI 239R-18 Ultra-High-Performance Concrete: An Emerging Technology Report. American Concrete Institute, 2018.
34. P. D. Sheet, "Sika ® CarboDur ® BC 8," no. October, pp. 8–10, 2023.
35. Pan B, Liu F, Zhuge Y, Zeng JJ, Liao J. ECCs/UHPFRCCs with and without FRP reinforcement for structural strengthening/repairing: a state-of-the-art review. Constr Build Mater. 2022;316:125824. https://doi.org/10.1016/j.conbuildmat.2021.125824.
36. C. A. E. User, "Abaqus theory manual," Abaqus 6.13 Doc., no. Dassault Systemes Simulia Corp., Providence, RI, USA., 2014.
37. GB, "National Standard of the People's Republic of China - Code for Design of Concrete Structures," Construction, vol. Beijing, pp. 64–73, 2002.
38. Jia L, Fang Z, Huang Z, Pilakoutas K, Wang Q, Tan X. Flexural behavior of uhpc beams prestressed with external cfrp tendons. Appl Sci. 2021;11(19):9189. https://doi.org/10.3390/app11199189.
39. Asadi M. Experimental Test and Finite Element Modelling of Pedestrian. Test, No. Figure. 2010;1:60876.
40. dos Santos LR, de Sousa CH, Caldas RB, Grilo LF. Finite element model for bolted shear connectors in concrete-filled steel tubular columns. Eng Struct. 2020;203:109863. https://doi.org/10.1016/j.engstruct.2019.109863.
41. Obaidat YT, Heyden S, Dahlblom O. The effect of CFRP and CFRP/concrete interface models when modelling retrofitted RC beams with FEM. Compos Struct. 2010;92(6):1391–8. https://doi.org/10.1016/j.compstruct.2009.11.008.
42. Ayough P, Sulong NR, Ibrahim Z. Analysis and review of concrete-filled double skin steel tubes under compression. Thin-Walled Struct. 2020;148:106495. https://doi.org/10.1016/j.tws.2019.106495.
43. Belakhdar K, Tounsi A. Finite element analysis of initially damaged beams repaired with FRP plates. Compos Struct. 2015;134:429–39. https://doi.org/10.1016/j.compstruct.2015.07.124.
44. Hawileh RA, Rasheed HA, Abdalla JA, Al-Tamimi AK. Behavior of reinforced concrete beams strengthened with externally bonded hybrid fiber reinforced polymer systems. Mater Des. 2014;53:972–82. https://doi.org/10.1016/j.matdes.2013.07.087.